SLAC–PUB–5421
UCRL-JC-106453
February 1991
(T/E)

Systematics of J/ψ Production in Nuclear Collisions*

R. Vogt

Lawrence Livermore National Laboratory
P. O. Box 808
Livermore, California 94550

and

S. J. Brodsky and P. Hoyer†

Stanford Linear Accelerator Center
Stanford University
Stanford, California 94309

We present a comprehensive QCD–based model for the x_f and nuclear dependences of heavy quarkonium production in photon–, hadron–, and nuclear–induced collisions. The calculated x_f dependence reflects both leading–twist QCD fusion subprocesses and higher–twist intrinsic heavy–quark components of the hadron wavefunction. A–dependent effects due to final–state absorption, interactions with comovers, shadowing of parton distributions, and intrinsic heavy–quark components are identified. The model is compared with data for J/ψ, ψ', and Υ production in pion–, proton–, and nucleus–nucleus collisions.

(Submitted to Nuclear Physics B)

*This work was supported by the U.S. Department of Energy under Contract No. W-7405-Eng-48 at LLNL and Contract No. DE-AC03-76SF00515 at SLAC.

†On leave from Department of High Energy Physics, University of Helsinki, SF–00170, Helsinki, Finland. Work supported by the Academy of Finland.

1. Introduction

The dependence of J/ψ production on the longitudinal momentum fraction, x_f, and on the size of the nuclear target are in striking conflict with conventional predictions of perturbative QCD. When comparing the x_f dependence of J/ψ production in heavy and light nuclear targets, increased absorption is observed in heavy relative to light targets at high x_f [1,2,3,4]. A strong absorptive component at high x_f is in complete disagreement with models of J/ψ production based only on parton fusion [5,6]. This behavior is particularly puzzling since, from formation time arguments, one would expect that large longitudinal momentum J/ψ's have less probability of being absorbed than those produced at $x_f \sim 0$, a trend observed in the p_T dependence of J/ψ production. The ratio of J/ψ production in heavy to light targets as a function of p_T is seen to increase with p_T, low-p_T J/ψ's being absorbed more readily [1,2,7]. The distribution of J/ψ's at large x_f in pion and proton-induced collisions as measured by NA3 is also too hard to be accounted for by the conventional fusion mechanisms assuming the usual gluon distributions. Mechanisms such as three gluon fusion [8] and inelastic initial-state scattering [9] do not adequately describe the x_f-dependent data. Clearly another explanation is needed.

The A dependence is conventionally parameterized by a power law as

$$\sigma_{hA\to\psi} = \sigma_{hN\to\psi} A^{\alpha} \ , \tag{1}$$

where $\sigma_{hN\to\psi}$ is the total J/ψ production cross section of hadron projectile h on a nucleon. NA3 reported $\alpha = 0.94 \pm 0.03$ for 200 GeV protons on Pt and H_2 targets integrated over all x_f [1]. However, as a function of x_f, α decreases from 0.97 at $x_f = 0$ to 0.7 at $x_f \to 1$ [1,2,3,10,11]. If J/ψ production were independent of the presence of nuclear matter, the production cross section would grow linearly with A.

In this work, we study a two-component explanation of the x_f dependence. The first component, dominant at moderate values of x_f, is the perturbative QCD model of parton fusion [12]. Taken literally, this hard-scattering approach would yield an approximately linear A dependence, as in dilepton production by the Drell-Yan mechanism. Some absorption should occur, leading to a less than linear A dependence of J/ψ production by parton fusion. Several effects contribute to the A dependence of parton fusion, including final-state interactions and nuclear shadowing of the target gluons and sea quarks. The second component of the x_f dependence is assumed to arise from an intrinsic heavy quark component of the projectile [13,14,15]. Since the charm quark mass is large, these quarks carry a significant fraction of the longitudinal momentum, contributing to the large x_f portion of the cross section. In this picture, the intrinsic $c\bar{c}$ state is of small spatial extent and passes through the target while the slower light quarks interact primarily on the nuclear surface, giving rise to a near $A^{2/3}$ dependence of intrinsic charm [15]. We will discuss each part of the model in detail in the subsequent sections.

Our starting point is the J/ψ production data of NA3 [1]. In their analysis, the

x_f dependent data was divided into two different pieces so that

$$\frac{d\sigma(\mathrm{H_2})}{dx_f} = \frac{d\sigma_h}{dx_f} + \frac{d\sigma_d}{dx_f} \tag{2}$$

$$\frac{d\sigma(\mathrm{Pt})}{dx_f} = A^{\alpha'}\frac{d\sigma_h}{dx_f} + A^{\beta}\frac{d\sigma_d}{dx_f} \; . \tag{3}$$

The 'hard' component, σ_h, with an $A^{0.972}$ dependence is attributed to parton fusion. We associate the 'diffractive' component, σ_d, exhibiting an $A^{0.71}$ dependence in pA collisions and an $A^{0.77}$ dependence in πA collisions, with intrinsic charm. The diffractive component, which mainly contributes at large x_f, cannot be accounted for by the usual leading twist, $\mathcal{O}(1/m_Q^2)$, perturbative QCD subprocesses. Taken together, these components give the effective α of eq. (1).

This paper is organized as follows. In sections 2 and 3 we describe the parton fusion model and each contribution to the A dependence of this model. We reproduce $d\sigma_h/dx_f$ as observed by NA3. In section 4 we discuss the intrinsic charm model and its A dependence. This intrinsic charm model is compared to the NA3 distributions of $d\sigma_d/dx_f$. We use pertinent experimental data to fix the parameters of our model. Once these parameters are set, in section 5 we compare our model to the x_f and A dependences of J/ψ production in the NA3 [1], E537 [2], E672 [16], and E772 [3,4] experiments. We also discuss the ψ' and Υ A dependences observed by E772 and their expected x_f dependences. Finally we make predictions for quarkonium production at RHIC under the assumption that no quark–gluon plasma is formed. These calculations may serve as a benchmark against which the future RHIC data may be compared to search for exotic effects. In section 6 we draw our conclusions.

2. The parton fusion model

The hadroproduction of heavy quarks in leading–twist perturbative QCD may be regarded as the sum of contributions from $q\bar{q}$ annihilation and gg fusion. The lowest order cross sections of these QCD subprocesses, averaged over initial spin and color, have been determined to be [12,17]

$$\sigma(q\bar{q} \to c\bar{c}; m^2) = \frac{8\pi\alpha_s^2}{27m^6}(m^2 + 2m_c^2)\lambda \tag{4}$$

$$\sigma(gg \to c\bar{c}; m^2) = \frac{\pi\alpha_s^2}{3m^6}\left\{(m^4 + 4m^2m_c^2 + m_c^4)\ln\left(\frac{m^2+\lambda}{m^2-\lambda}\right) - \frac{1}{4}(2m^2 + 31m_c^2)\lambda\right\} \; , \tag{5}$$

where m is the invariant mass of the $c\bar{c}$ pair, m_c is the charm quark mass, and $\lambda = \sqrt{m^4 - 4m^2m_c^2}$. We use $m_c = 1.5$ GeV in our calculations. The strong coupling constant is taken as

$$\alpha_s(m^2) = \frac{12\pi}{(33 - 2n_f)\ln(m^2/\Lambda^2)} \; . \tag{6}$$

The number of active flavors, n_f, is 4. The cutoff, Λ, is fixed at 0.2 GeV, and the mass scale is set at $m = m_{J/\psi}$.

Let x_p be the fractional momentum carried by the projectile partons and x_t be the fractional momentum of the target partons. We introduce the functions $G_p(x_p)$, $q_{pi}(x_p)$, $\bar{q}_{pi}(x_p)$ and $G_t(x_t)$, $q_{ti}(x_t)$, $\bar{q}_{ti}(x_t)$, the gluon, quark, and antiquark distribution functions within the projectile and target hadrons respectively. The quark flavors are labeled by the subscript i. The hadroproduction cross section is then described, according to the QCD factorization theorem, as a convolution of the quark–antiquark annihilation and gluon–gluon fusion cross sections. In section 3.3 we will modify the structure functions to account for the presence of nuclear matter. We introduce the function [17]

$$\begin{aligned} H_{pt}(x_p, x_t; m^2) &= G_p(x_p)G_t(x_t)\sigma(gg \to c\bar{c}; m^2) \\ &\quad + \sum_{i=u,d,s} (q_{pi}(x_p)\bar{q}_{ti}(x_t) + \bar{q}_{pi}(x_p)q_{ti}(x_t))\sigma(q\bar{q} \to c\bar{c}; m^2) \ , \end{aligned} \quad (7)$$

where we sum over light quark flavors relevant to $c\bar{c}$ production. If y is the $c\bar{c}$ rapidity in the center of mass frame and $\sqrt{s}$ is the center of mass energy, the differential cross section for free $c\bar{c}$ production by parton fusion is

$$\frac{d\sigma_h}{dm^2 dy}(pt \to c\bar{c}; m^2) = \frac{1}{s} H_{pt}(x_p, x_t; m^2) \ . \quad (8)$$

The invariant mass of the pair may be related to the total energy in the nucleon–nucleon center of mass frame through $m^2 = x_p x_t s = \tau^2 s$. The momentum fractions x_p and x_t are related to the rapidity through $x_{p,t} = \tau \exp(\pm y)$, and to the forward momentum fraction of the $c\bar{c}$ pair by $x_f = x_p - x_t$. We now change variables to x_f and τ so that

$$\frac{d\sigma_h}{d\tau dx_f} = \frac{2\tau}{\sqrt{x_f^2 + 4\tau^2}} H_{pt}(x_p, x_t; x_p x_t s) \ , \quad (9)$$

where $x_{p,t} = \frac{1}{2}(\pm x_f + \sqrt{x_f^2 + 4\tau^2})$.

To apply this cross section to the production of $c\bar{c}$ bound states, we must integrate the free production cross section over τ from the $c\bar{c}$ production threshold, $\tau_1 = 2m_c/\sqrt{s}$, to the open charm threshold, $\tau_2 = 2m_D/\sqrt{s}$. Then

$$\frac{d\sigma_h}{dx_f} = 2F \int_{\tau_1}^{\tau_2} \tau d\tau \frac{H_{pt}(x_p, x_t; x_p x_t s)}{\sqrt{x_f^2 + 4\tau^2}} \ , \quad (10)$$

where F is the fraction of the bound state production cross section attributed to J/ψ production; at this point it must be regarded as a parameter of the fusion model. Since the η_c, η_c', $\chi_{0,1,2}$, and ψ' resonances also lie in the range $2m_c \leq m \leq 2m_D$, we might expect $F \leq 1/7$ in hadroproduction. Both direct and indirect J/ψ production from decays of higher mass charmonium resonances are included in F. This may introduce a weak energy dependence. Contributions to the fusion cross section

from higher order subprocesses in α_s have been calculated [18]. These contributions affect the normalization of $d\sigma_h/dx_f$ and therefore may be absorbed into F. In our description of the NA3 hard distributions between 150 and 280 GeV, F varies from $1/5 - 1/8$ for J/ψ production by pions and $F \sim 1/9$ for proton production. In fig. 1, we show $Bd\sigma_h/dx_f$ for π^- beams at all energies as well as π^+ and p beams at 200 GeV [1]. The branching ratio to $\mu^+\mu^-$ pairs, B, is included since this is the detected J/ψ decay channel. Note that all NA3 cross sections are given as $B\sigma$, rather than a total production cross section.

The parton fusion model as described here does not predict the p_T dependence of J/ψ production. The p_T of the J/ψ is determined from the intrinsic p_T dependence of the partons and higher–order perturbative QCD contributions. We do not consider the high–p_T dependence of J/ψ production in this work; it has been described in *e.g.* Refs. [19,20] and references contained therein. Thus this description is only valid for kinematic regions where the J/ψ p_T is small [17].

We will use this model to describe ψ' and Υ production as well. For the ψ', we use $m = m_{\psi'}$ while in Υ production, $n_f = 5$, $m_c \to m_b = 4.5$ GeV, and $m_D \to m_B = 5.28$ GeV. In each case, the fraction F is adjusted to account for differences in the number of available production channels and the branching ratios to muon pairs, the observed decay channel. For example, since the more massive ψ' can only be produced directly, its F is much smaller than that of the J/ψ.

The parton structure functions contained in eq. (7) were determined by NA3 from a fit to the σ_h data at $Q^2 = m_\psi^2$ [1]. As usual, one assumes that the sea quark distribution satisfies $q_s(x) = \bar{q}_s(x)$ and that the scaling property $\bar{u}_s(x) = \bar{d}_s(x) = 2\bar{s}_s(x)$ holds for both π and p projectiles. The valence quarks of the proton are normalized to satisfy $\int_0^1 dx\, u_v(x) = 2$ and $\int_0^1 dx\, d_v(x) = 1$ while the valence quarks of the pion must satisfy $\int_0^1 dx\, v_\pi(x) = 2$. Assuming u, d, and s valence and sea quarks in the proton leads to the momentum sum $\int_0^1 dx\, x(u_v + d_v + G + 2(u_s + d_s + s_s)) = 1$. The total u quark content of the proton is then $u = u_v + u_s$ while $d = d_v + d_s$. The quark content of a $\pi^-(d\bar{u})$, on the other hand, leads to $\bar{u} = v_\pi + \bar{u}_s$ and $d = v_\pi + d_s$ and inversely for $\pi^+(u\bar{d})$. The shape of the gluon distribution in the proton, $G \propto (1-x)^{n_p}$, was determined to give $n_p = 5.2$ from a fit of $d\sigma_h/dx_f$ to incident protons and $B\sigma(\bar{p})/B\sigma(p)$. A fit to the incident pion data using the gluon distribution of the nucleon target gave $n_\pi = 2.4$. The normalizations of the gluon distributions were determined from the fraction of the projectile momentum carried by the gluons.

The parton structure functions have recently been analyzed to next–to–leading order in QCD using all the available data from deep–inelastic scattering measurements of the proton structure function along with recent prompt photon and Drell–Yan production data [21]. Using these distributions leads to a 5% difference in the size of F but makes no qualitative change in the shape of $d\sigma_h/dx_f$. We now discuss the contributions to the A dependence of the parton fusion model.

3. A dependence of parton fusion

Our model of the A dependence in the low–x_f region, where the parton fusion contributions dominate, includes both initial– and final–state effects. At low x_t, shadowing of the sea quarks and gluons in the target may lead to a change in the initial parton densities. A depletion in the nuclear parton densities would mean that fewer low–x_t partons are available for heavy flavor production. This effect becomes more important with increasing beam energies where smaller x_t's are probed. After the $c\bar{c}$ pair has been produced, it may be absorbed by nucleons in the target and interact with secondary particles produced in the collision and comoving with the pair [22]. The probability of nuclear absorption decreases with energy, whereas comover production grows with energy, increasing the importance of comover interactions. In a realistic model of J/ψ production in hadron–nucleus, hA, and nucleus–nucleus, A_1A_2, collisions, all these effects should be included since each contributes at a level varying with the kinematic regime studied. We examine the A dependence of each of these effects in detail and describe how the model parameters are determined from available J/ψ production data. One should keep in mind that the bulk of the integrated A dependence arises from the small–x_f region.

3.1 Nuclear absorption of the J/ψ

The $c\bar{c}$ pair may suffer interactions with nucleons and be absorbed before it can escape the target. The pair, produced as a color singlet in a hard collision, is initially of small spatial extent, $\propto m_c^{-1}$, on the order of its production time. The proper time required for the formation of the charmonium bound state, τ_ψ, is considerably longer. While the $c\bar{c}$ pair is expanding to its bound state size, it is moving through the target. Consequently, depending on the initial energy of the projectile and the size of the target, the $c\bar{c}$ pair may form a J/ψ inside or outside of the target. The effectiveness of nuclear absorption thus depends on the time–dependent size of the $c\bar{c}$ pair. The $c\bar{c}$–N absorption cross section may be expected to grow as a function of proper time until τ_ψ, saturating at the asymptotic value $\sigma_{\psi N}$. This may explain why high energy photoproduction experiments using the vector–meson dominance model to describe J/ψ production arrive at an absorption cross section of 1–2 mb.

We simulate the growth of the absorption cross section by [23,24]

$$\sigma_{\rm abs}(z'-z) = \begin{cases} \sigma_{\psi N}\left(\dfrac{\tau}{\tau_\psi}\right)^\kappa & \text{if } \tau < \tau_\psi \\ \sigma_{\psi N} & \text{otherwise} \end{cases} . \tag{11}$$

The exponent κ measures the increase of $\sigma_{\rm abs}$ during hadronization of the $c\bar{c}$ pair. If $\sigma_{\rm abs}$ is proportional to the geometric cross section, πd^2, then we expect $\kappa \sim 2$. For a quantum mechanical treatment, see ref. [6]. In the usual Glauber scattering models, where the J/ψ is assumed to be instantaneously produced, $\kappa = 0$, giving rise to the A^α parameterization. This form of the cross section depends upon the $c\bar{c}$

pair being produced as a color singlet. Octet $c\bar{c}$ pairs would interact immediately to produce D mesons and thus correspond to $\kappa = 0$ in eq. (11).

The effect of nuclear absorption alone on the J/ψ production cross section in hA collisions may be expressed as

$$\sigma_{hA\to\psi} = \sigma_{hN\to\psi} \int d^2b\, T_A^{\rm eff}(b) \ , \tag{12}$$

where $T_A^{\rm eff}(b)$ is the effective nuclear profile function

$$T_A^{\rm eff}(b) = \int_{-\infty}^{\infty} dz\, \rho_A(b,z) \exp\left\{ -\int_z^{\infty} dz' \rho_A(b,z') \sigma_{\rm abs}(z'-z) \right\} \ . \tag{13}$$

The exponential factor is the nuclear absorption survival probability of the $c\bar{c}$ pair and ρ_A is the nuclear density profile. The proper time τ is related to the path length traversed by the $c\bar{c}$ pair through nuclear matter, $\tau = (z'-z)/\gamma v$.

Assuming, for illustrative purposes, that the nuclear target has a uniform density profile, $\rho_A = 3/(4\pi r_0^3)$, we can analytically estimate $\sigma_{\psi N}$ from low–energy photoproduction data. Integrating over the volume of the nucleus and taking into account the growth of $\sigma_{\rm abs}$, we have [24,27]

$$\frac{\sigma_{hA\to\psi}}{A\sigma_{hN\to\psi}} \approx \exp\left\{ -\frac{9\sigma_{\psi N}}{4\pi r_0^2} A^{1/3} f(r) \right\} \ , \tag{14}$$

with

$$f(r) = \begin{cases} Cr^{\kappa} & ; \ \text{for } r \le 1, \\ \dfrac{1}{r^4}\left\{ \dfrac{r^4-1}{4} - \dfrac{2\kappa(r^3-1)}{3\kappa+3} + \dfrac{\kappa(r^2-1)}{2\kappa+4} + C \right\} & ; \ \text{for } r \ge 1, \end{cases} \tag{15}$$

where $r = 2R_A/\gamma v \tau_\psi$ and $C = 2\{(\kappa+1)(\kappa+2)(\kappa+4)\}^{-1}$. When $r \le 1$, the $c\bar{c}$ pair is still expanding, becoming a fully–formed J/ψ when $r > 1$. If we choose $\kappa = 0$, $f(r)$ is independent of A, and, since $A^{1/3} \approx \ln A$ for large A, the usual Glauber result is regained. Note that the reference to a fully–formed J/ψ applies only to the low x_f behavior. The Lorentz time dilation is large at high x_f, leading to an increase in the hadronization time. Consequently, fast J/ψ's are usually formed outside the target, as described in section 4.

To determine $\sigma_{\psi N}$, we turn to the SLAC photoproduction data of ref. [25]. Although the $c\bar{c}$ production mechanism, photon–gluon fusion, is different than that in hadroproduction, it is still relevant to deduce $\sigma_{\psi N}$ from this data since the $c\bar{c}$ pair, once produced, will be absorbed the same way regardless of the production mechanism. In this experiment, a 20 GeV photon beam was directed on Be and Ta targets. No comoving secondaries are expected in photoproduction, shadowing effects are negligible at this energy, and there is no intrinsic charm in the projectile photon. Thus this experiment provides a pure determination of $\sigma_{\psi N}$. Assuming

that $\kappa = 0$ and $\sigma_{\psi N}$ is small, eq. (14) may be expanded to lowest order in $\sigma_{\psi N}$ to find

$$\frac{A_{\rm eff}}{A} = 1 - \frac{9\sigma_{\psi N} A^{1/3}}{16\pi r_0^2} \ , \tag{16}$$

where $A_{\rm eff} = \sigma_{\gamma A \to \psi}/\sigma_{\gamma N \to \psi}$. From the SLAC measurement, $\sigma({\rm Be})/\sigma({\rm Ta}) = 1.21 \pm 0.07$, a ψ–N absorption cross section, $\sigma_{\psi N} = 3.5 \pm 0.8$ mb, can be obtained from the solution of eq. (16). To fix $\sigma_{\psi N}$ for an expanding system, we use the more general expression

$$\frac{A_{\rm eff}}{A} = 1 - \frac{9\sigma_{\psi N} A^{1/3}}{4\pi r_0^2} f(r) \ . \tag{17}$$

In the relatively low energy SLAC experiment, $r > 1$ in both targets so that the J/ψ interacts with its full absorption cross section. This experiment thus provides an upper bound on the ψ–N absorption cross section. Using $\kappa = 2$ and $\tau_\psi = 0.9$ fm, we determine $\sigma_{\psi N} \approx 5$ mb. In a more general calculation using diffuse nuclear shapes with $\sigma_{\psi N} = 5$ mb, we find $\sigma({\rm Be})/\sigma({\rm Ta}) = 1.23$, well within the experimental range. We will thus use $\sigma_{\psi N} = 5$ mb in our further calculations.

3.2 Interactions with comoving secondaries

Comoving secondaries, formed at a time $\tau_0 \sim 1 - 2$ fm after hadronic collisions, consistent with soft particle production, may also scatter with the $c\bar{c}$ pair. A spectator hadron moving with a velocity similar to the c and $\bar{c}$ quarks will enhance the probability of forming charmed hadrons at the expense of charmonium production. In contrast to color transparency effects in the absorption of $Q\overline{Q}$ systems in nuclei, the comover interaction is independent of whether or not the $c\bar{c}$ pair is produced as a color octet or singlet. The probability that the $c\bar{c}$ pair survives to create the J/ψ after interactions with comovers is [24,27]

$$S \approx \exp\left\{ - \int d\tau \, \langle \sigma_{\rm co} v \rangle n(\tau, b) \right\} \ , \tag{18}$$

where σ_{co} is the $c\bar{c}$–comover absorption cross section, $v \sim 0.6$ is the relative velocity of the $c\bar{c}$ with the comovers, and $n(\tau, b)$ is the density of comovers at time τ and impact parameter b. Integrating over time τ and relating the initial density of the system to the final hadron rapidity density through the use of scaling dynamics [26], one finds [24,27]

$$\int d\tau n(\tau, b) \approx \frac{1}{\pi R^2} \ln\left(\frac{\tau_f}{\tau_0}\right) \frac{dN}{dy}|_{y=y_c} \sigma_{hN} T_A(b) \ , \tag{19}$$

where τ_f is the effective proper lifetime over which the comovers can interact with the $c\bar{c}$ pair, and $dN/dy|_{y=y_c}$ is the central rapidity density. We use the estimate

$\tau_f \sim R/c_s$ where R is the projectile radius and $c_s \sim 1/\sqrt{3}$ is the transverse velocity of sound in the nuclear frame. The shape of the rapidity density in inclusive J/ψ production for pA collisions is unknown. However, there is some evidence of a rapidity plateau in inclusive pA data [28], therefore we assume that the central rapidity density is constant over the reduced rapidity range of the produced J/ψ's. High–x_f J/ψ's produced in the tail of the rapidity distribution suffer few comover interactions. However, $d\sigma_h/dx_f$ is significantly reduced in this region, decreasing the importance of this effect. Since the transverse area from which comovers are produced is approximately equal to the total hadron–nucleon cross section, the survival probability in hA collisions may be recast as

$$S(b) \approx \exp\left\{-\langle\sigma_{\rm co} v\rangle \frac{dN}{dy}|_{y=y_c} \ln\left(\frac{\tau_f}{\tau_0}\right) T_A(b)\right\} \ . \tag{20}$$

Since $T_A(b) = \int_{-\infty}^{\infty} dz \rho(b,z) \propto A^{1/3}$, this leads to the Glauber result. Thus comover interactions do not introduce any unusual A dependence. The rapidity density grows with center of mass energy as $dN/dy|_{y=y_c} \sim as^{\delta}$ where a and δ are constants which can be determined from data [29].

The growth of rapidity density with energy implies an increasingly important role for comovers in the A dependence. Meanwhile, the nuclear absorption survival probability of the pair is approaching unity with increasing energy since at ultra-relativistic energies, $\tau < 1$ for all nuclear targets. Given our parameters, comover interactions become the dominant final–state effect at an incident energy of $\sim$ 1 TeV [24].

To determine $\sigma_{\rm co}$, we turn to the transverse energy dependence of J/ψ production in nucleus–nucleus collisions as measured by NA38 [30,31]. In order to understand the E_T dependence, we must consider the survival probability as a function of the nuclear impact separation B. Comovers make a significant contribution to the E_T dependence of the A_1A_2 data since the rapidity density is proportional to the global transverse energy, E_T, of the system [32,33,34]. Expressing the survival probability for comover interactions as a function of E_T, we write

$$S(E_T;B) = \exp\left\{-\left(\frac{\langle\sigma_{\rm co} v\rangle}{\mathcal{A}(B)} \frac{dN}{dy}|_{y=y_c} \ln\left(\frac{\tau_f(B)}{\tau_0}\right)\right) \frac{E_T(B)}{E_T(0)}\right\} \ . \tag{21}$$

where $\tau_0 \sim 2$ fm, the time for the production of secondaries, and $\mathcal{A}(B)$ is the area of nuclear overlap. We use central O+U collisions as a baseline for $dN/dy|_{y=y_c}$ and $E_T(0)$ and assume that their ratio remains fixed for all CERN experiments discussed.

In order to compare with the NA38 data and determine $\sigma_{\rm co}$, we must form the ratio of the E_T–dependent production cross sections

$$Y(E_T) = \frac{d\sigma_{A_1A_2\to\psi}/dE_T}{d\sigma_{A_1A_2\to\mu\mu}/dE_T} \ . \tag{22}$$

where $\sigma_{A_1A_2\to\psi}$ is the J/ψ production cross section in A_1A_2 collisions and $\sigma_{A_1A_2\to\mu\mu}$ represents the production cross section of continuum muon pairs. Experimentally [30],

$$Y(E_T) = \frac{dN_\psi/dE_T}{dN_{\mu\mu}/dE_T} \ , \tag{23}$$

is obtained by dividing the J/ψ and continuum data into E_T bins.

The E_T–dependent J/ψ production cross section is calculated from [24]

$$\frac{d\sigma_{A_1A_2\to\psi}}{dE_T} = \sigma_{NN\to\psi}\int d^2B\int d^2b\, T^{\rm eff}_{A_1}(b)T^{\rm eff}_{A_2}(B-b)p(E_T;B)S(E_T;B) \ , \tag{24}$$

where $T^{\rm eff}_{A_1}$ and $T^{\rm eff}_{A_2}$ take into account the survival probability for a J/ψ produced at impact parameter b. The probability for E_T to be produced at nucleus–nucleus impact parameter B, $p(E_T;B)$, is assumed to be [35]

$$p(E_T;B) = \frac{1}{\sqrt{2\pi\Delta(B)}}\exp\left\{-\frac{(E_T-\overline{E}_T(B))^2}{2\Delta(B)}\right\} \ . \tag{25}$$

We take $\overline{E}_T(B) = \epsilon_0 N(B)$, where $N(B)$ is the number of participant nucleons and ϵ_0 is the energy per collision participant, and $\Delta(B) = \epsilon_0\omega\overline{E}_T(B)$, where ω determines the fluctuation of E_T at a given B. The participant model of nuclear collisions suggests that ϵ_0 and ω are independent of the target and projectile masses [27], thus we use the same ϵ_0 and ω to describe all the NA38 E_T distributions. The J/ψ production cross section on a nucleon, $\sigma_{NN\to\psi}$, has been calculated by integrating over the NA38 x_f acceptance. The experimental x_f acceptance [36], $-0.03 < x_f < 0.18$, is in a region where the intrinsic charm content of the nucleon is very small and an energy regime where the effect of shadowing is negligible.

Two factors in the J/ψ–comover survival probability $S(E_T;B)$, $\tau_f(B)$ and $\mathcal{A}(B)$, are a function of nuclear impact parameter in A_1A_2 collisions. Only in central collisions with complete nuclear overlap can we simply take $\tau_f(B) = R_{A_1}/c_s$ and $\mathcal{A}(B) = \pi R^2_{A_1}$, where R_{A_1} is the radius of the smaller nucleus. We assume that the lifetime of the dense system only plays a role in J/ψ production if $\tau_f > \tau_0$ since $\tau_f < \tau_0$ implies that the J/ψ is interacting weakly with the comovers. Thus in A_1A_2 collisions τ_f is defined for $\tau_f > \tau_0$ as

$$\tau_f = \begin{cases} R_{A_1}/c_s & B < R_{A_2} - R_{A_1} \\ (R_{A_1} + R_{A_2} - B)/(2c_s) & R_{A_2} - R_{A_1} < B < R_{A_2} + R_{A_1} \end{cases} \ . \tag{26}$$

When $\tau_f < \tau_0$, the survival probability for J/ψ–comover interactions is set to unity. The area of nuclear overlap is also calculated as a function of B, decreasing in peripheral collisions.

The production cross section of continuum muon pairs within the J/ψ mass region as a function of E_T is

$$\frac{d\sigma_{A_1A_2\to\mu\mu}}{dE_T} = \sigma_{NN\to\mu\mu}\int d^2B\int d^2b\, T_{A_1}(b)T_{A_2}(B-b)p(E_T;B) \ . \tag{27}$$

Note that $\int d^2B \int d^2b T_{A_1} T_{A_2} = A_1 A_2$. Since muons only interact through the electroweak force, there is no absorption by hadrons. We have assumed that the continuum arises only from Drell–Yan production in order to calculate $\sigma_{NN\to\mu\mu}$. Other muon sources such as $K^{\pm}$ and $\pi^{\pm}$ decays and semileptonic decays of charmed hadrons are also present. Instead of calculating all the contributions, we normalize our calculation of $Y(E_T)$ to the yield in the center of the lowest E_T bin of the data.

The solid curve in fig. 2(a) shows our calculation of $Y(E_T)$ in O+U collisions at $\sqrt{s} = 19.4$ GeV with $\sigma_{\rm co} = 2$ mb. This value of $\sigma_{\rm co}$ gives a reasonable description of the E_T dependence. Three E_T regions can be clearly seen. At low E_T, corresponding to large B, comovers play no role since $\tau_f < \tau_0$. In the intermediate E_T region, corresponding to peripheral collisions, comovers play an increasingly important role as B decreases. High E_T central collisions involve complete nuclear overlap with constant τ_f and $\mathcal{A}$. The nuclear absorption survival probability, contained in $T_{A_1}^{\rm eff}$ and $T_{A_2}^{\rm eff}$ is not directly a function of E_T and results in a rather flat E_T distribution arising from $p(E_T;B)$ alone, as shown in the dashed curve of fig. 2(a) with $\sigma_{\rm co} = 0$. For $\sigma_{\rm co} > 2$ mb, the E_T dependence becomes too strong. The NA38 data from S+U and O+Cu collisions are shown in fig. 2(b)–(c) along with our calculation. These results from nucleus–nucleus collisions lead us to use $\langle \sigma_{\rm co} v \rangle = 1.2$ mb in our further calculations.

The trends of the nucleus–nucleus data are consistent with the presence of comovers. It is not surprising that $\sigma_{\rm co} < \sigma_{\psi N}$ since the J/ψ–comover interaction, at low relative velocity, is a threshold process while J/ψ–N interactions occur at high momentum. We now turn to low–x_t shadowing, an initial–state effect that modifies the parton distribution functions in nuclear matter.

3.3 Shadowing of sea quarks and gluons

The term shadowing refers to the fact that parton distributions in a nucleus are depleted below simple additivity at low values of x_t. In a moving frame, the nucleus has a longitudinal size $\Delta z \approx 2R_A m/p$ where R_A is the nuclear radius, m is the proton mass, and p is the nucleon momentum. The longitudinal size of a sea quark or gluon with momentum k_z within a nucleon is $\Delta z \approx 1/k_z$. When the size of the nucleon components becomes larger than the size of the nucleus itself, $1/k_z > 2R_A m/p$ or $x_t < 1/(2R_A m)$, the sea quarks and gluons from different nucleons overlap spatially and may be considered nuclear rather than nucleon constituents. Hence partons from different nucleons along the same impact parameter can interact to reduce the large density and cause shadowing at low x_t. A specific quantum mechanical model for this reduction is given in ref. [37]. We will follow the estimates of ref. [38] to incorporate gluon shadowing into our model.

The nuclear sea quark and gluon distributions may be defined in terms of their nucleon counterparts as

$$\frac{1}{A} x_t q_s^A(x_t) \;=\; x_t q_s(x_t) R_s(x_t, A) \tag{28}$$

$$\frac{1}{A}x_t G^A(x_t) \;=\; x_t G(x_t) R_g(x_t, A)\;, \tag{29}$$

where R_s and R_g include all information on nuclear shadowing at low Q^2. Following the above discussion, shadowing arises due to interactions between low x_t partons from two different nucleons that overlap longitudinally. Thus the onset of nuclear shadowing occurs when partons exceed the size of nucleons in the nucleus or equivalently the distance between neighboring nucleons at $x_t < x_n = 1/(2rm) = 0.1$. Shadowing increases as more partons overlap, saturating when the partons are completely overlapping at $x_t = x_A = 1/(2R_A m)$. Thus $R_{s,g}$ must be unity when $x_n < x_t < 1$ and at a minimum when $x_t < x_A$. In the range $x_A \leq x_t \leq x_n$, $R_{s,g}$ decreases proportional to the amount of parton overlap

$$R_{\rm over} = \frac{1/x_t - 1/x_n}{1/x_A - 1/x_n}\;. \tag{30}$$

The A dependence of shadowing is approximately given by $A^{1/3}-1$ due to correction terms in the evolution equations of the parton distributions. These corrections arise from the interaction of small-x_t gluons from two different nucleons. Given this A dependence we choose the shadowing factors $R_{s,g}$ to be

$$R_{s,g}(x_t, A) = \begin{cases} 1 & x_n < x_t < 1 \\ 1 - K_{s,g}(A^{1/3}-1)R_{\rm over} & x_A < x_t < x_n \\ 1 - K_{s,g}(A^{1/3}-1) & 0 < x_t < x_A \end{cases}\;. \tag{31}$$

We neglect the effects of shadowing on the valence quark distributions. In ref. [38], K_s was set to 0.1 from a study of virtual photon cross sections measured in deep-inelastic scattering off nuclei. We take this value of K_s in our further calculations.

Fig. 3 illustrates some of the qualitative effects of gluon shadowing in the energy regime of E772 [3], where $\tau = 0.081$, as a function of x_f with $x_t = (-x_f + \sqrt{x_f^2 + 4\tau^2})/2$. In fig. 3(a), we plot $R_g(x_t, A)$ in a tungsten target for $K_g = 0$, 0.005, 0.05, and 0.1. We now illustrate the shadowing effect on the nuclear gluon distribution function. In fig. 3(b), $(1/A)x_t G^A(x_t)$ is given for a tungsten target at $K_g = 0$, 0.005, 0.05, and 0.1. Fig. 3(c) shows $(1/A)x_t G^A(x_t)$ for H, C, Cu, and W nuclei at $K_g = 0.05$. We fix $K_g = 0.05$ from a comparison of our model with the E772 data (see section 5).

The shadowing effect, like comover interactions, becomes more important to the A dependence with increasing energy since x_t decreases correspondingly. Shadowing should be most important at high x_f since the lowest x_t's are probed in this region. However, as we shall see, its effect on the overall x_f dependence is rather weak, having an approximately 15% effect on the E772 x_f dependent ratios. This weak dependence arises from the small fusion contribution to the production cross section at high x_f and the near additivity of the A dependence of parton fusion. Another $c\bar{c}$ production mechanism, important at high x_f, is necessary to describe the x_f dependence of the J/ψ production data consistently. We now turn to a description of

the intrinsic charm content of the projectile, leading to enhanced $c\bar{c}$ production at high x_f, in an effort to more fully understand the x_f dependence of J/ψ production.

4. Intrinsic charm of the projectile

QCD predicts that the hadronic wavefunction of the projectile contains virtual heavy–quark pairs with a higher twist suppressed probability $\mathcal{O}(1/m_Q^2)$. These heavy quarks must carry the largest fraction of the projectile momentum in order to keep the bound state together [13,14,15],

$$\langle x_Q \rangle > \langle x_q \rangle \ , \tag{32}$$

thus implying an important contribution to charm production at large x_f. As in the leading twist processes, charmonium production is a small fraction of the open charm cross section. For each Fock state of the hadron, momentum conservation implies $\sum_i \vec{k}_{\perp i} = 0$ and $\sum_i x_i = 1$, where $k_{\perp i}$ and x_i are the transverse momentum and fractional longitudinal momentum carried by each constituent. The state is off the hadron energy shell by an amount $\epsilon \propto m_h^2 - \sum_{i=1}^n ((\vec{k}_\perp^2 + m^2)/x)_i$ where m_h is the hadron mass and m_i is the mass of each of the constituent partons. The general form of the Fock state wavefunction is

$$\Psi(\vec{k}_{\perp i}, x_i) = \frac{\Gamma(\vec{k}_{\perp i}, x_i)}{m_h^2 - \sum_{i=1}^n ((\vec{k}_\perp^2 + m^2)/x)_i} \ , \tag{33}$$

where Γ is a vertex function that must be obtained from a nonperturbative calculation. One expects Γ to be a decreasing function of the off–shell variable ϵ. This wavefunction is appropriate to a projectile moving with large momentum at fixed equal time, or, more generally, in any frame at fixed light–cone time. In the limit of zero binding energy, Ψ is singular and the fractional momenta peak at $x_i = m_i/m$. Note that the denominator is minimized when the heaviest constituents carry the largest fraction of the longitudinal momentum. This is equivalent to the notion that the constituents of a moving bound state have the same rapidity. As a representative form, we choose the differential cross section for intrinsic charm corresponding to the n–particle Fock state (integrated over $k_{\perp i}$) [13,14]

$$\frac{d\sigma}{dx_1 \ldots dx_n} = N_n \frac{\delta(1 - \sum_{i=1}^n x_i)}{(m_h^2 - \sum_{i=1}^n (\hat{m}_i^2/x_i))^2} \ , \tag{34}$$

where $\hat{m}_i = \sqrt{\langle \vec{k}_{\perp i}^2 \rangle + m_i^2}$ is the average transverse mass and N_n is a normalization factor. According to eq. (33), we expect the average squared transverse momentum $\langle k_\perp^2 \rangle$ to be proportional to the square of the quark mass. The inverse square power in eq. (34) is chosen to correspond to typical higher–twist components involving two valence quark interactions, including the $(1/m_Q^2)$ suppression in the cross section due to the resolution of the intrinsic heavy quarks [39].

Turning to $|uudc\bar{c}\rangle$, the intrinsic charm state of the proton, we denote $\hat{m}_c = \hat{m}_4$, $\hat{m}_{\bar{c}} = \hat{m}_5$, and assign $\hat{m}_{1,2,3}$ to the valence quarks. We assume the effective values $\hat{m}_c = \hat{m}_{\bar{c}} = 1.8$ GeV and $\hat{m}_{1,2,3} = 0.45$ GeV. In this work, we are interested in the x_f distribution of the intrinsic $c\bar{c}$ state:

$$\frac{d\sigma(p)}{dx_f} = \int \prod_{i=1}^{5} dx_i \frac{d\sigma}{dx_1 \ldots dx_5} \delta(x_f - x_c - x_{\bar{c}}) \; . \tag{35}$$

The integrals over the delta functions are trivial, leaving us with

$$\begin{aligned} \frac{d\sigma(p)}{dx_f} &= N_5 \int_0^{x_f} dx_c \int_0^{1-x_f} dx_2 \int_0^{1-x_f-x_2} dx_3 \left(m_p^2 - \hat{m}_c^2 \left(\frac{1}{x_c} + \frac{1}{x_f - x_c} \right) \right. \\ &\quad \left. - \hat{m}_q^2 \left(\frac{1}{x_3} + \frac{1}{x_2} + \frac{1}{1 - x_2 - x_3 - x_f} \right) \right)^{-2} \; . \end{aligned} \tag{36}$$

After a change of variables, we have

$$\begin{aligned} \frac{d\sigma(p)}{dx_f} &= N_5 x_f^3 (1 - x_f)^4 \int_0^1 \prod_{i=1}^{3} dy_i (1 - y_2) \left(x_f (1 - x_f) m_p^2 - \frac{(1 - x_f)\hat{m}_c^2}{y_3 (1 - y_3)} \right. \\ &\quad \left. - x_f \hat{m}_q^2 \left(\frac{1}{y_2} + \frac{1}{y_1 (1 - y_2)} + \frac{1}{(1 - y_1)(1 - y_2)} \right) \right)^{-2} \; . \end{aligned} \tag{37}$$

The average x_f of the $c\bar{c}$ bound state within the proton is $\langle x_f \rangle = 0.51$.

Similarly, for the intrinsic charm state of the pion, the integrations over x_i yield

$$\begin{aligned} \frac{d\sigma(\pi)}{dx_f} &= N_4 x_f^3 (1 - x_f)^3 \int_0^1 \prod_{i=1}^{2} dy_i \left(x_f (1 - x_f) m_\pi^2 - \frac{(1 - x_f)\hat{m}_c^2}{y_2 (1 - y_2)} \right. \\ &\quad \left. - \frac{x_f \hat{m}_q^2}{y_1 (1 - y_1)} \right)^{-2} \; , \end{aligned} \tag{38}$$

with $\langle x_f \rangle = 0.62$. The lower power of $1 - x_f$ in the pion cross section results from integrating over two light quark momenta rather than three.

We now identify $d\sigma/dx_f$ with the 'diffractive' cross section $d\sigma_d/dx_f$ of NA3. The differential cross section has a m_c^{-4} dependence, down by a factor of m_c^2 from that of the parton model. In fig. 4, we show $Bd\sigma_d/dx_f$ from the NA3 experiment [1] using eqs. (37) and (38) to calculate the J/ψ x_f distribution for the p and π beams respectively. The agreement of the measured 'diffractive' components with the predictions of the above intrinsic charm model in the proton and pion appears reasonable. The pion normalization was set from the ratio, $\sigma_d/\sigma(\mathrm{H_2}) = 0.18$, determined by NA3. For the proton beam, we have recalculated the normalization leaving out the first two low-x_f data points, making $\sigma_d/\sigma(\mathrm{H_2}) = 0.125$, rather than 0.29 as in ref. [1]. We are not able to explain the low-x_f data using intrinsic charm. We assume that the ratios $\sigma_d/\sigma(\mathrm{H_2})$ are energy independent.

We will briefly discuss the expected A dependence of the intrinsic charm model. Recall that the intrinsic $c\bar{c}$ state is closer to being on shell when the charm quarks

carry large x_i. Also, the transverse size of the $c\bar{c}$ system is small, $\sim m_c^{-1}$ [15]. Provided that the produced $c\bar{c}$ state is a color singlet, it can penetrate the target with little energy loss. The light quarks of the state, however, are of typical hadronic size and moving slowly in relation to the heavy quarks. Thus the light quarks will interact on the nuclear surface while the $c\bar{c}$ pair passes through the target. It is the surface interaction of the light quarks from which the A dependence of intrinsic charm arises, leading to an approximate $A^{2/3}$ dependence.

To specify the A dependence of 'diffractive' J/ψ production, NA3 used the model of ref. [40] to constrain β in eq. (3). The effective nucleon number N is expressed as

$$N(A;\sigma_1,\sigma_2) = \frac{1}{\sigma_2 - \sigma_1} \int d^2b \, (e^{-\sigma_1 T_A(b)} - e^{-\sigma_2 T_A(b)}) \; , \tag{39}$$

where $\sigma_{1,2}$ is the total cross section for particle 1, 2 incident on a nucleon. Each nuclear target then has its own value of β, defined as

$$\beta = \frac{\ln N(A;\sigma_1,\sigma_2)}{\ln A} \; . \tag{40}$$

Using $\sigma_1 = 24$ mb for π beams and $\sigma_1 = 39$ mb for p beams and $\sigma_2 = 0$ for the J/ψ gives $\beta = 0.77$ for pions and 0.71 for protons on a Pt target. This procedure is consistent with the intrinsic charm model. Therefore β is an A dependent quantity but has no inherent energy dependence. Increasing the size of the target decreases β. The exponent β thus represents the 'diffractive' production of J/ψ's while α' of eq. (3) refers to final–state interactions. Since the change in β with A is small, we will use the β's fixed by NA3.

5. Results

We now have a comprehensive model with which we can confront the nuclear dependence of the J/ψ production cross section in photon–, hadron–, and nucleus–induced processes. The main effects are shadowing of the parton distributions, nuclear absorption, comover interactions, and the 'diffractive' intrinsic charm component. We rewrite eq. (3) to more clearly illustrate where each component enters into the A and x_f dependences

$$\frac{d\sigma(A)}{dx_f} = A^{\alpha'} \frac{d\sigma_h^A}{dx_f} + A^{\beta} \frac{d\sigma_d}{dx_f} \; . \tag{41}$$

The A dependence of nuclear shadowing, an initial–state effect in the leading–twist cross section, is contained in σ_h^A. The two final–state processes, nuclear absorption and comover interactions, give an effective reduction of the linear A dependence expected from hard scattering alone, expressed as

$$A^{\alpha'} = \int d^2b \, T_A^{\rm eff}(b) S(b) \; , \tag{42}$$

where $T_A^{\rm eff}(b)$ is defined in eq. (13) and $S(b)$ is defined in eq. (20). In the case of the intrinsic charm component, σ_d, β is set at 0.77 for incident pions and 0.71 for protons. The ratio $\sigma_d/\sigma(\mathrm{H_2})$ remains energy independent.

We can now use the E772 data to determine the amount of gluon shadowing required by our model. Thus given $\sigma_{\psi N}$, $\langle\sigma_{\rm co}v\rangle$, and $\sigma_d/\sigma(\mathrm{H_2})$, we can fix the size of K_g. We take $K_s = 0.1$ and use the 800 GeV pA J/ψ production data of E772 [3] to fix K_g. At 800 GeV, $\tau = m_\psi/\sqrt{s} = 0.081$ and, given the experimental acceptance, $0.1 < x_f < 0.65$, x_t lies within the shadowing regime, $0.01 < x_t < 0.045$. In fig. 5, we show the E772 data normalized to the deuterium target. We assume that the effects of nuclear absorption and comover interactions are negligible in the deuterium nucleus. The dot–dashed curve shows $K_g = 0$, the result when shadowing is not included. The dashed curve shows our calculation if the comover interaction were ignored, $\sigma_{\rm co} = 0$, but including shadowing with $K_g = 0.05$ and $K_s = 0.1$. The solid line is our result including both shadowing and comover interactions. We use $K_g = 0.05$ and $K_s = 0.1$ in further calculations.

If we chose a larger $\sigma_{\rm co}$, we could describe the data with little or no nuclear shadowing. However, this would cause the NA38 E_T dependence to be too strong. Likewise, gluon shadowing alone could also provide an approximate description of the E772 A dependence. However, the NA38 experiment, with $\tau = 0.16$ and $0.06 < x_t < 0.16$, requires comovers. Since shadowing is not E_T dependent, it cannot explain the NA38 data. Clearly both effects are needed for a consistent description of these data sets. Therefore, our parameters are fixed at $\sigma_{\psi N} = 5$ mb, $\kappa = 2$, $\tau_\psi = 0.9$ fm, $\langle\sigma_{\rm co}v\rangle = 1.2$ mb, $K_s = 0.1$, and $K_g = 0.05$.

We now can confront the NA3 A and x_f dependent data. In fig. 6, we present the A dependence of the πA and pA data [1] along with our model calculations. Fig. 7 illustrates the size of the x_f dependent effects in the 200 GeV proton data. Fig. 7(a) demonstrates the change in $d\sigma(\mathrm{H_2})/d\sigma(\mathrm{Pt}) \equiv (d\sigma(\mathrm{H_2})/dx_f)/((1/A)d\sigma(\mathrm{Pt})/dx_f)$ induced by leaving out any one of the components of the model. The solid curve shows the net result of all effects. The main non–additive nuclear effect is due to intrinsic charm. In this low–energy data, shadowing is relatively unimportant even at large x_f since the intrinsic charm component dominates in this region. Fig. 7(b) shows $Bd\sigma_h/dx_f$ (solid curve) and $Bd\sigma_d/dx_f$ (dashed curve) on the same scale to illustrate the relative size of the components of the cross section more effectively. Fig. 8 gives the x_f dependence of all the NA3 data. Note in fig. 8(a) that there is only a slight difference in the x_f dependence due to the change in incident energy. The difference in J/ψ production by π^+ and π^- beams at 200 GeV in fig. 8(b) is due to the different parton distributions of the oppositely charged pions. The main effect is the stronger A dependence in the proton–induced reaction. For $x_f \to 1$, $d\sigma(\mathrm{H_2})/d\sigma(\mathrm{Pt}) \sim A^{1-\beta}$. Note also that the x_f dependence of the nuclear ratio for proton beams begins to increase at a smaller value of x_f than that of the pion at the same energy due to the different shapes of the intrinsic charm distributions in eqs. (37) and (38).

A comparison of our model with the E537 125 GeV $\pi^- A$ data [2] is shown in fig.

9. It was this data, with its anomalous A dependence, that led the authors of ref. [23] to suggest a cross section growing with proper time as in eq. (11). This data was also the basis of the study in ref. [24]. Attempts to model only this data using final–state absorption alone resulted in a $\sigma_{\psi N}$ significantly larger than the upper limit set by photoproduction[1] [23,24].

In fig. 9(a), we have normalized our calculation of σ/A to the beryllium target. Our overall absolute cross section is about 15% too high. There are two reasons why this discrepancy might exist. There may be unaccounted for differences in experimental acceptance in our calculation. More importantly, it has been pointed out that hydrogen is not a good target to fix the A dependence of a process, especially if only two targets are used [42,43]. In the determination of the A dependence of $\pi^{\pm}$, $K^{\pm}$, p, and $\overline{p}$ production on multiple nuclei, the hydrogen production data consistently exceeded that expected from the extrapolation from heavy to light nuclear production [42]. Since we have modeled the H_2 target of NA3, the resulting production cross sections may be somewhat high in comparison with experiments not using a hydrogen target. The normalization is not a problem when the data is presented in the form of a ratio, such as the E772 normalization to deuterium. In fact, deuterium may be a better target to use in A–dependence studies than hydrogen [43].

The solid curve in fig. 9(a) shows our result for $\kappa = 2$ while the dashed curve is a calculation with $\kappa = 0$, $\sigma_{\psi N} = 3.5$ mb, and $\sigma_{co} = 0$. The A dependence is slightly steeper when using $\kappa = 0$. At low x_f, no formation time effects occur and the J/ψ interacts with its total absorption cross section from the instant of production. Note however that $\kappa = 0$ is inconsistent with observed hadronization effects in jet fragmentation [44] and color transparency studies [22,45,46]. The x_f dependent ratios in fig. 9(b), $d\sigma(\mathrm{W})/d\sigma(\mathrm{Be})$ (solid curve) and $d\sigma(\mathrm{W})/d\sigma(\mathrm{Cu})$ (dashed curve), as predicted by the model, give only a fair description of the data. More absorption is present at high x_f here than expected from the NA3 data, possibly due to increased nuclear absorption in tungsten. We would predict the correct magnitude of the ratios at $x_f = 0$ if our A–dependent calculation also described the tungsten data.

Next we present a comparison of our model with the data of the recent Fermilab experiment E672 [16]. A 530 GeV π^- beam was directed on C, Al, Cu, and Pb targets. The A– and x_f–dependent data are shown in fig. 10 along with our model calculations. Again the overall normalization is not quite exact, as explained before. Note that the lead target does not show any anomalous absorption as do tungsten targets in other experiments, evidently since lead is a very stable nucleus. Our model does an adequate job of describing the data in the acceptance region $0.1 \leq x_f \leq 0.8$.

We now turn to a more complete description of the E772 data, including ψ' and

[1]It is possible that there is more absorption in the tungsten nucleus due to its superdeformed shape [41]. This could also account for the trend in the E772 data (see fig. 5). Attempts to model the E537 data without accounting for the deformed shape of tungsten might result in an anomalously large $\sigma_{\psi N}$.

Υ production [3,4]. Since shadowing is an initial–state effect, it is unaffected by the type of resonance produced. However, the other components of the model must be examined for potential heavy–quark mass dependences.

It has been suggested that the hadron–nucleon absorption cross section varies with the size of the incident hadron as [47,48]

$$\sigma_{hp} \propto R_h^2 R_p^2 \; . \tag{43}$$

This implies that in relation to $\sigma_{\psi N}$, the absorption cross section of higher–lying quarkonium states may be expressed as

$$\sigma_{RN} = \sigma_{\psi N} \left(\frac{R_R}{R_\psi} \right)^2 \; . \tag{44}$$

The radii of the ψ' and Υ have been calculated from nonrelativistic potential models [49]. From these calculations, one predicts $\sigma_{\psi' N} = 3.7\, \sigma_{\psi N}$ and $\sigma_{\Upsilon N} = 0.25\, \sigma_{\psi N}$. The formation times, $\tau_R \sim R_R / v_{Q\overline{Q}}$ are different also. Since the ψ' is larger, it has a longer formation time than the J/ψ, $\tau_{\psi'} = 1.5$ fm. The smaller and more massive Υ has a shorter formation time, $\tau_\Upsilon = 0.76$ fm [49].

The magnitude of the comover cross section depends on the probability that the produced Q or $\overline{Q}$ quark interact with comoving spectators before the quarkonium bound state can be formed. We thus expect that the $c\bar{c}$–comover interaction cross section is the same for the J/ψ and ψ' bound states. To a first approximation, we expect the cross section to depend only on the velocity of the heavy quark and not on its mass [50]. The proper time of interaction, τ_f, could depend on the particular quarkonium state, but this is only a logarithmic effect. Thus it is plausible that

$$\sigma_{\rm co}(\psi) = \sigma_{\rm co}(\psi') \simeq \sigma_{\rm co}(\Upsilon) \; . \tag{45}$$

As an alternative, we will also consider the possibility that the Υ–comover cross section may be reduced from the ψ–comover cross section in proportion to the heavy–quark masses so that

$$\sigma_{\rm co}(\Upsilon) = \sigma_{\rm co}(\psi) \left(\frac{m_c}{m_b} \right)^2 \; . \tag{46}$$

We have compared both these possibilities with the E772 Υ A dependence.

Intrinsic charm and intrinsic beauty have essentially the same x_f–dependent production cross sections since the forms of eqs. (37) and (38) do not change except in replacement of m_c with m_b. However, the percentage of intrinsic heavy quark states within the projectile changes. We can assume that the ratio $\sigma_d/\sigma(\mathrm{H_2})$ remains the same for J/ψ and ψ' production. However, the percentage of intrinsic $b\bar{b}$ states present decreases in proportion to the square of the quark mass [14], resulting in

$$\frac{\sigma_d}{\sigma(\mathrm{H_2})}|_\Upsilon = \left(\frac{m_c}{m_b} \right)^2 \frac{\sigma_d}{\sigma(\mathrm{H_2})}|_\psi \; . \tag{47}$$

Since these quarkonium states are formed well outside the nucleus at high x_f, the intrinsic heavy quark component of the cross section has the same A dependence.

Fig. 11 shows the result of these changes on the ψ' and Υ A dependence compared to the data of E772 [3,4]. The calculated ψ' A dependence in fig. 11(a) very closely resembles that of the J/ψ, due to the reduced role of nuclear absorption at high energies (see section 3.2). Since $\sigma_{\rm co}$ remains unchanged, there is little difference between the J/ψ and ψ' A dependences even though $\sigma_{\psi' N} \sim 4\sigma_{\psi N}$. The Υ A dependence is illustrated in fig. 11(b). The solid curve shows the result with $\sigma_{\rm co}(\Upsilon)$ as in eq. (45) while the dashed curve uses $\sigma_{\rm co}(\Upsilon)$ from eq. (46). It is obvious that $\sigma_{\rm co}(\Upsilon) \simeq \sigma_{\rm co}(\psi)$ yields a better description of the A–dependent data. Intrinsic beauty plays a negligible role in the A dependence since $\sigma_d/\sigma({\rm H_2})|_\Upsilon \sim 0.01$.

In fig. 12, we compare the predictions of the complete model to the E772 x_f–dependent data [3]. Gluon shadowing, comover interactions, and intrinsic charm each play a role. Absorption is negligible in this high momentum data. The decreasing nuclear yield at large x_f is mainly due to the intrinsic charm component, as seen in $d\sigma({\rm Fe})/d\sigma({\rm D})$. In the model, the effects of comovers and shadowing are both important at small x_f where parton fusion is dominant. The predicted increase in the slope of $d\sigma(A)/d\sigma(D)$ exhibited by the model is due to the assumed form of the A dependence of the gluon shadowing model. An important check of the consistency of our approach is that the normalized A dependence and the x_f dependence of J/ψ and ψ' production are essentially identical. This would not be true in a model without any formation time effects. Shadowing plays a negligible role in the Υ data since $\tau = m_\Upsilon/\sqrt{s} = 0.25$. Given the same x_f acceptance for Υ and J/ψ production, the x_t range is $0.17 < x_t < 0.2$, too high for shadowing to be important. Intrinsic beauty has little effect on the A dependence, and would only be apparent in a careful measurement of the Υ distribution at $x_f > 0.6$. At the present time no data is available in this region.

Fig. 13 shows our calculation of J/ψ production in O+U collisions in comparison to our prediction for ψ' production in the same experiment. The J/ψ and ψ' will suffer different nuclear absorption effects at low x_f. However, this absorption has a very small effect on the shape of the E_T distribution. The magnitudes of $Y(E_T)/Y(23)$ for the J/ψ and ψ' are very similar since $\sigma_{\rm co}(\psi) = \sigma_{\rm co}(\psi')$. Thus the ratio of J/ψ to ψ' production should show little E_T dependence. The absolute magnitude of the E_T–integrated ratio is ~ 70. The NA38 experiment detected the ψ' and may have data on $Y(E_T)$ as a function of E_T for the ψ'.

Finally we use our model to predict the behavior of quarkonium production at RHIC, the heavy–ion collider to be built at Brookhaven. These calculations may serve as a benchmark against which the future data can be compared in a search for new effects. Fig. 14(a) shows the predicted A dependence in 100 GeV on 100 GeV pA collisions. We first present the A dependence of the J/ψ production cross section. At $\tau = m_\psi/\sqrt{s} = 0.015$ and $x_f = 0$, the nuclear shadowing contribution is quite important, large enough to be experimentally confirmed or ruled out. The solid curve shows our full result whereas the dashed curve results from a calculation

without shadowing. There is a 25% difference in σ/A with and without shadowing at high A. (The ψ' results are similar.) We also show predictions for Υ production in pA collisions in the dot–dashed curve. Our curves have been normalized to $A = 1$ to facilitate direct comparison of the J/ψ and Υ dependences.

Intrinsic beauty may be a factor in the A and x_f dependence of Υ production at RHIC. Fig. 14(b) shows a calculation of the J/ψ and Υ x_f–dependent ratios, $\sigma(\mathrm{Au})/\sigma(\mathrm{H})$, in 100 + 100 GeV pA collisions. The x_f range possible at RHIC depends on the detector mass and rapidity acceptances. If we assume that $y = 3$ is the maximum accepted rapidity, as in the proposed dimuon spectrometer, then $x_{f_{\mathrm{max}}} = 0.3$ for J/ψ production in 100 + 100 GeV collisions. Thus $0.0007 < x_t < 0.015$, deep in the shadowing region. All of the J/ψ x_f dependence will therefore arise from shadowing since the intrinsic charm component is small within the x_f–acceptance range. Since the Υ is more massive, a maximum rapidity of $y = 3$ means that $x_{f_{\mathrm{max}}} = 0.95$. Thus RHIC can cover the entire x_f range of Υ production even at the maximum energy of the collider, suggesting a role for intrinsic beauty at large x_f. Shadowing is important in Υ production since $\tau = 0.047$ and $x_t < 0.047$, but not as strong as for J/ψ production. The solid curve is our prediction for J/ψ production. (The ψ' result is identical.) The Υ production ratio is shown in the dot–dashed curve. Note the steep fall–off due to shadowing in the low–x_f region.

Fig. 14(c) shows the predicted E_T dependence of J/ψ production in 100 + 100 GeV Au+Au collisions at RHIC with comover interactions (the solid curve) and without (the dashed curve). The presence or absence of shadowing only changes the normalization—not the shape of the curve. The dramatic hadronic effects shown here highlight the need for systematic studies of quarkonium production at RHIC.

6. Conclusions

We have examined J/ψ, ψ', and Υ production over a wide range of energies. Our model includes nuclear absorption, comover scattering, initial–state nuclear shadowing, and intrinsic heavy–quark states in the projectile. All of these effects contribute to an overall picture of the x_f, A, and E_T dependences of quarkonium production in hadron–nucleus and nucleus–nucleus collisions. The importance of each contribution depends on the kinematic regime studied.

It is important that each of the model components be examined in detail experimentally. We believe that we have developed a plausible set of model parameter values, but these parameter values should be systematically tuned in experiments that kinematically isolate each production component. For example, other experiments should divide the x_f–dependent data into two components as NA3 did to search for a diffractive component in the cross section. This could confirm the existence of intrinsic heavy–quark states. The production cross sections should be presented as a function of x_f for each target, rather than in a ratio which can distort the importance of particular effects. Shadowing should be investigated more

thoroughly to better determine the size of the gluon contribution. Experiments at RHIC, with its variable energy and beam capabilities, should be able to study shadowing in detail. The low x_f–production behavior will help clarify the trade–off between nuclear absorption and comover interactions with increasing energy. Studies of nuclear collisions will better fix σ_{co} as well.

It is clear that all of the above A dependent effects must be considered in a complete QCD description of J/ψ and Υ production. All the contributions we have examined in our model will be present in the 'background' of ultrarelativistic heavy–ion collisions. In particular, it is necessary to understand J/ψ production in detail to search for exotic effects such as quark–gluon plasma production.

We would like to thank M. Gyulassy, P. V. Ruuskanen, G. Miller, P. McGaughey, and S. Gavin for helpful discussions. R. Vogt would also like to thank the Institute for Nuclear Theory in Seattle and the Nuclear Theory Group at LBL for hospitality. P. Hoyer is grateful to the SLAC Theory Group for its hospitality during his sabbatical.

References

[1] J. Badier *et al.*, Z. Phys. **C20** (1983) 101.

[2] S. Katsanevas *et al.*, Phys. Rev. Lett. **60** (1988) 2121.

[3] D. M. Alde *et al.*, Phys. Rev. Lett. **66** (1991) 133.

[4] J. Moss, in proceedings of the 8th International Conference on Ultrarelativistic Nucleus–Nucleus Collisions, Menton, France, 1990, to be published in Nucl. Phys. **A**.

[5] P. Hoyer, M. Vänttinen, and U. Sukhatma, Phys. Lett. **246B** (1990) 217.

[6] J. Hüfner and M. Simbel, Universität Heidelberg preprint.

[7] P. Bordalo *et al.*, Phys. Lett. **193B** (1987) 373.

[8] L. Clavelli, P. H. Cox, B. Harms, and S. Jones, Phys. Rev. **D32** (1985) 612.

[9] B. Z. Kopeliovich and F. Niedermayer, 1984 Dubna Preprint JINR-E2-84-834.

[10] Y. U. Antipov *et al.*, Phys. Lett. **76B** (1978) 235.

[11] M. J. Corden *et al.*, Phys. Lett. **110B** (1982) 415.

[12] V. Barger, W. Y. Keung, and R. N. Phillips, Phys. Lett. **91B** (1980) 253.

[13] S. J. Brodsky, P. Hoyer, C. Peterson, and N. Sakai, Phys. Lett. **93B** (1980) 451.

[14] S. J. Brodsky, C. Peterson, and N. Sakai, Phys. Rev. **D23** (1981) 2745.

[15] S. J. Brodsky and P. Hoyer, Phys. Rev. Lett. **63** (1989) 1566.

[16] S. Kartik *et al.*, Phys. Rev. **D41** (1990) 1.

[17] V. Barger, W. Y. Keung, and R. N. Philips, Z. Phys. **C6** (1980) 169.

[18] P. Nason, S. Dawson, and R. K. Ellis, Nucl. Phys. **B303** (1988) 607.

[19] S. Gavin and M. Gyulassy, Phys. Lett. **214B** (1988) 241.

[20] J. Hüfner, Y. Kurihara, and H. J. Pirner, Phys. Lett. **215B** (1988) 218.

[21] P. N. Harriman, A. D. Martin, W. J. Stirling, and R. G. Roberts, Phys. Rev. **D42** (1990) 798.

[22] S. J. Brodsky and A. H. Mueller, Phys. Lett. **206B** (1988) 685.

[23] J.-P. Blaizot and J.-Y. Ollitrault, Phys. Lett. **217B** (1989) 386.

[24] S. Gavin and R. Vogt, Nucl. Phys. **B345** (1990) 104.

[25] R. L. Anderson *et al.*, Phys. Rev. Lett. **38** (1977) 263.

[26] J. D. Bjorken, Phys. Rev. **D27** (1983) 140.

[27] R. Vogt, Ph. D. thesis, State University of New York at Stony Brook, 1989, unpublished.

[28] R. J. Ledoux, Nucl. Phys. **A498** (1989) 205c.

[29] V. E. Barnes, Nucl. Phys. **A498** (1989) 193c.

[30] C. Baglin *et al.*, Phys. Lett. **220B** (1989) 471.

[31] J.-Y. Grossiord *et al.*, Nucl. Phys. **A498** (1989) 249c.

[32] R. Albrect *et al.*, Z. Phys. **C38** (1988) 3.

[33] J. Schukraft, Z. Phys. **C38** (1988) 59.

[34] A. Bamberger *et al.*, Z. Phys. **C38** (1988) 89.

[35] G. Baym, G. Friedman, and I. Sarcevic, Phys. Lett. **219B** (1989) 205.

[36] C. Gerschel, in proceedings of the International Workshop on Quark–Gluon Plasma Signatures, Strasbourg, France, 1990, Orsay preprint IPNO–DRE 90-24.

[37] S. J. Brodsky and H. J. Lu, Phys. Rev. Lett. **64** (1990) 1342.

[38] J. Qiu, Nucl. Phys. **B291** (1987) 746.

[39] S. J. Brodsky, J. C. Collins, S. D. Ellis, J. F. Gunion, and A. H. Mueller, in *Proceedings of the Summer Study on the Design and Utilization of the Superconducting Super Collider*, Snowmass, CO, 1984, edited by R. Donaldson and J. Morfin (Division of Particles and Fields of the American Physical Society, New York, 1985).

[40] K. S. Kölbig and B. Margolis, Nucl. Phys. **B6** (1968) 85.

[41] R. W. Hasse and W. D. Myers, *Geometrical Relationships of Macroscopic Nuclear Physics*, Springer Verlag, 1988.

[42] P. Stevenson and H. Miettinen, Phys. Lett. **214B** (1988) 241.

[43] W. Geist, in proceedings of the 8$^{\text{th}}$ International Conference on Ultrarelativistic Nucleus–Nucleus Collisions, Menton, France, 1990, to be published in Nucl. Phys. **A**.

[44] P. B. Renton, in *Proceedings of the Topical Conference on Nuclear Chromodynamics*, Argonne, IL, 1988, edited by J. Qiu and D. Sivers, World Scientific, 1988.

[45] G. R. Farrar, H. Liu, L. L. Frankfurt, and M. I. Strickman, Phys. Rev. Lett. **61** (1988) 686.

[46] B. K. Jennings and G. A. Miller, preprint 40427–20–N90, submitted to Phys. Rev. **D**.

[47] B. Povh and J. Hüfner, Phys. Rev. Lett. **58** (1987) 1612.

[48] J. F. Gunion and D. E. Soper, Phys. Rev. **D15** (1977) 2617 and references therein.

[49] F. Karsch and R. Petronzio, Z. Phys. **C37** (1988) 627.

[50] N. Weis, Phys. Rev. **D43** (1991) 810.

Figure Captions

Figure 1. The NA3 data on $Bd\sigma_h/dx_f$ for: (a) 200 GeV p, (b) 150 GeV π^-, (c) 200 GeV π^+, (d) 200 GeV π^-, and (e) 280 GeV π^- beams [1]. The solid curves are obtained from eq. (10).

Figure 2. We fix $\sigma_{co} = 2$ mb from an examination of the NA38 (a) O+U, (b) S+U, and (c) O+Cu J/ψ production data at $\sqrt{s} = 19.4$ GeV [31]. The solid curves represent our calculation using eq. (22). We also show a calculation with $\sigma_{co} = 0$ in fig. 2(a).

Figure 3. We display some qualitative effects of low–x_t shadowing. Fig. 3(a) shows R_g, defined in eq. (31), as a function of x_f for $A = 184$ and $\tau = 0.081$. We use $K_g = 0$, 0.005, 0.05, and 0.1. Fig. 3(b) uses the same parameters as above to display the nuclear gluon distribution of eq. (29) as a function of x_f for $K_g = 0$, 0.005, 0.05, and 0.1. Fig. 3(c) gives $(1/A)x_t G^A(x_t)$ as a function of x_f using $K_g = 0.05$ and $\tau = 0.081$ for $A = 1$, 12, 63, and 184.

Figure 4. The NA3 data on $Bd\sigma_d/dx_f$ [1] is compared with the calculated intrinsic charm x_f distributions in p and π projectiles of eqs. (37) and (38). Figs. (a), (b), and (c) are from the π data at 150, 280, and 200 GeV respectively, from eq. (38). Fig. (d) compares the p data at 200 GeV with a calculation using eq. (37).

Figure 5. We fix K_g using the E772 J/ψ production data [3]. The solid curve shows the result using $\sigma_{\psi N} = 5$ mb, $\kappa = 2$, $\langle \sigma_{co} v \rangle = 1.2$ mb, and $K_g = 0.05$. This should be contrasted with calculations including no shadowing (the dot–dashed curve) and no comover interactions (the dashed curve).

Figure 6. The A dependence of the NA3 experiment [1] is compared with our model calculations using eq. (41). Note that the cross sections are given as $B\sigma/A$, in terms of the branching ratio to muon pairs, rather than as total cross sections. To obtain the absolute production cross section, divide by the branching ratio $B(J/\psi \to \mu^+\mu^-) = 6.9\%$.

Figure 7. An illustration of the x_f–dependent effects on 200 GeV proton–induced J/ψ production. Fig. (a) displays the differences in the ratio $d\sigma(\mathrm{H_2})/d\sigma(\mathrm{Pt})$ caused by omitting certain parts of the calculation. The solid curve shows the complete model, the dashed curve shows the result without shadowing, the dot–dashed curve the result without comovers, and the dotted curve the result without intrinsic charm. Fig. (b) shows the x_f distributions of $B\sigma_h$ and $B\sigma_d$, along with the data, plotted on the same scale for better comparison.

Figure 8. The x_f–dependent data of NA3 [1]. Fig. (a) compares our model with π^- induced J/ψ production at 150 GeV (solid curve) and 280 GeV (dashed curve).

Fig. (b) compares 200 GeV J/ψ production by π^- (solid curve), π^+ (dashed curve), and p (dot–dashed curve) beams with our calculations.

Figure 9. The A and x_f dependent data of E537 [2]. Fig. (a) shows σ/A as a function of A using $\kappa = 2$, $\sigma_{\psi N} = 5$ mb, and $\langle \sigma_{\rm co} v \rangle = 1.2$ mb (the solid curve) and $\kappa = 0$, $\sigma_{\psi N} = 3.5$ mb, and $\langle \sigma_{\rm co} v \rangle = 0$ (dashed curve). Both curves are normalized to the Be point for comparison. Fig. (b) gives the x_f dependence of the ratios $d\sigma({\rm W})/d\sigma({\rm Be})$ (solid curve) and $d\sigma({\rm W})/d\sigma({\rm Cu})$ (dashed curve).

Figure 10. The A and x_f dependent data of E672 [16]. Fig. (a) displays σ/A as a function of A while fig. (b) displays the x_f dependence of the ratio $d\sigma({\rm Pb})/d\sigma({\rm C})$.

Figure 11. We show the A dependence of ψ', and Υ, as determined by E772 [4]. Both calculations are normalized to deuterium. We illustrate two different approximations to $\sigma_{\rm co}(\Upsilon)$ in fig. (b). The first, $\sigma_{\rm co}(\Upsilon) = \sigma_{\rm co}(\psi)$, is shown in the solid curve, and the second, $\sigma_{\rm co}(\Upsilon) = \sigma_{\rm co}(\psi)(m_c/m_b)^2$, is given by the dashed curve.

Figure 12. The E772 x_f–dependent data [3]. Model calculations are shown for the ratios $d\sigma({\rm C})/d\sigma({\rm D})$, $d\sigma({\rm Ca})/d\sigma({\rm D})$, $d\sigma({\rm Fe})/d\sigma({\rm D})$, and $d\sigma({\rm W})/d\sigma({\rm D})$, along with the data. In fig. (c) we show our model with certain pieces omitted. The solid curve is the full model, the dashed curve is without shadowing, the dot–dashed without comovers, and the dotted without intrinsic charm. In fig. (d) we also estimate the x_f dependence of Υ production, the dashed and dot–dashed curves using $\sigma_{\rm co}(\Upsilon)$ from eqs. (45) and (46) respectively.

Figure 13. We make a prediction for the NA38 O+U ψ' production data. The ratios $Y(E_T)/Y(23)$ for J/ψ (solid curve) and ψ' (dashed curve) production are shown together for comparison.

Figure 14. Model predictions for quarkonium production at RHIC. Fig. (a) shows the A dependence of J/ψ production at the highest RHIC energy with (solid curve) and without nuclear shadowing (dashed curve). The A dependence of Υ production is estimated in the dot–dashed curve. All curves are normalized to the pp production cross section. Fig. (b) shows the x_f–dependent ratio $d\sigma({\rm Au})/d\sigma({\rm H})$ for J/ψ (solid curve) and Υ (dashed curve) production. Fig. (c) illustrates the E_T dependence of J/ψ production with (solid line) and without (dashed line) comovers, both normalized to $E_T = 0$.

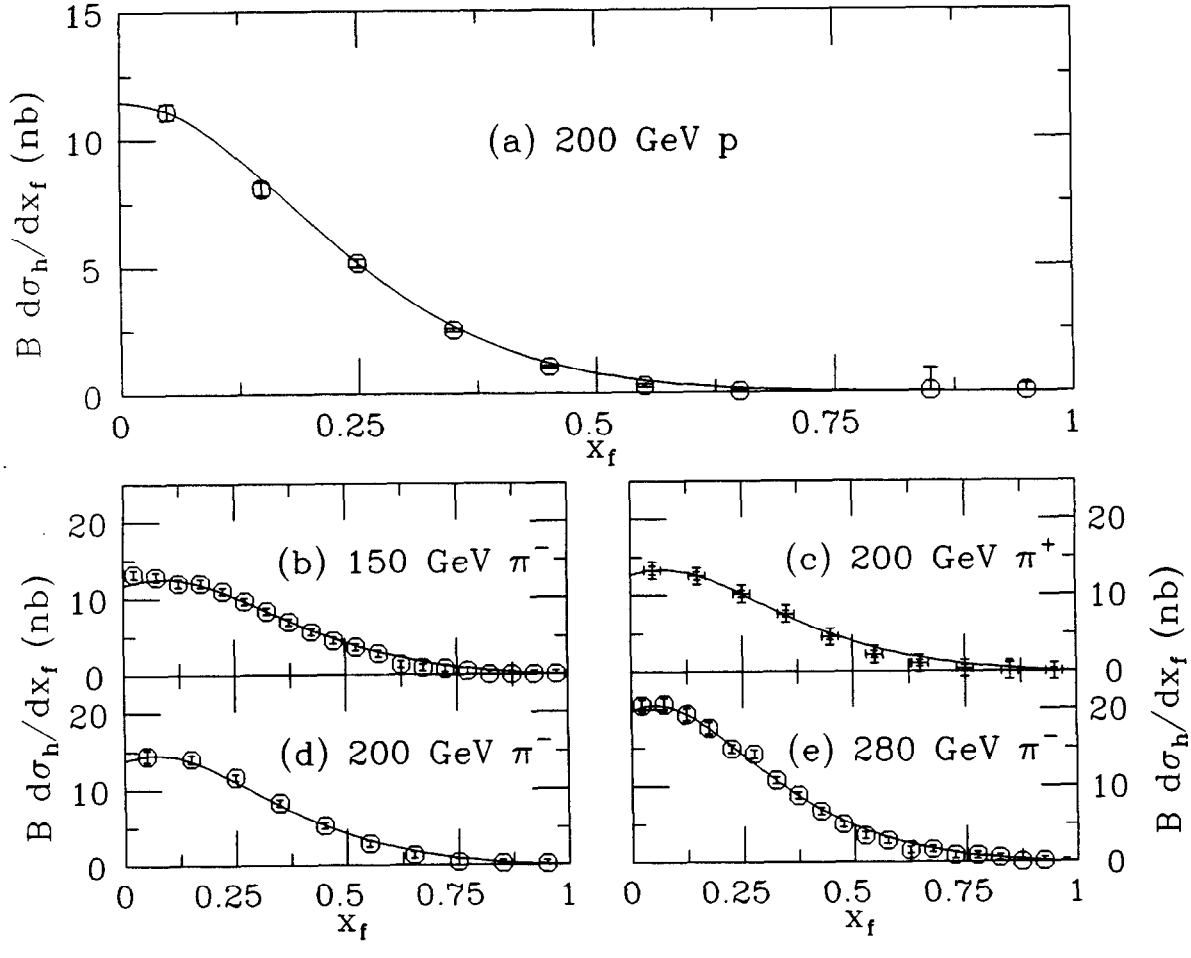
(a) 200 GeV p
(b) 150 GeV π^-
(c) 200 GeV π^+
(d) 200 GeV π^-
(e) 280 GeV π^-
B $d\sigma_h/dx_f$ (nb)
x_f

Fig. 1

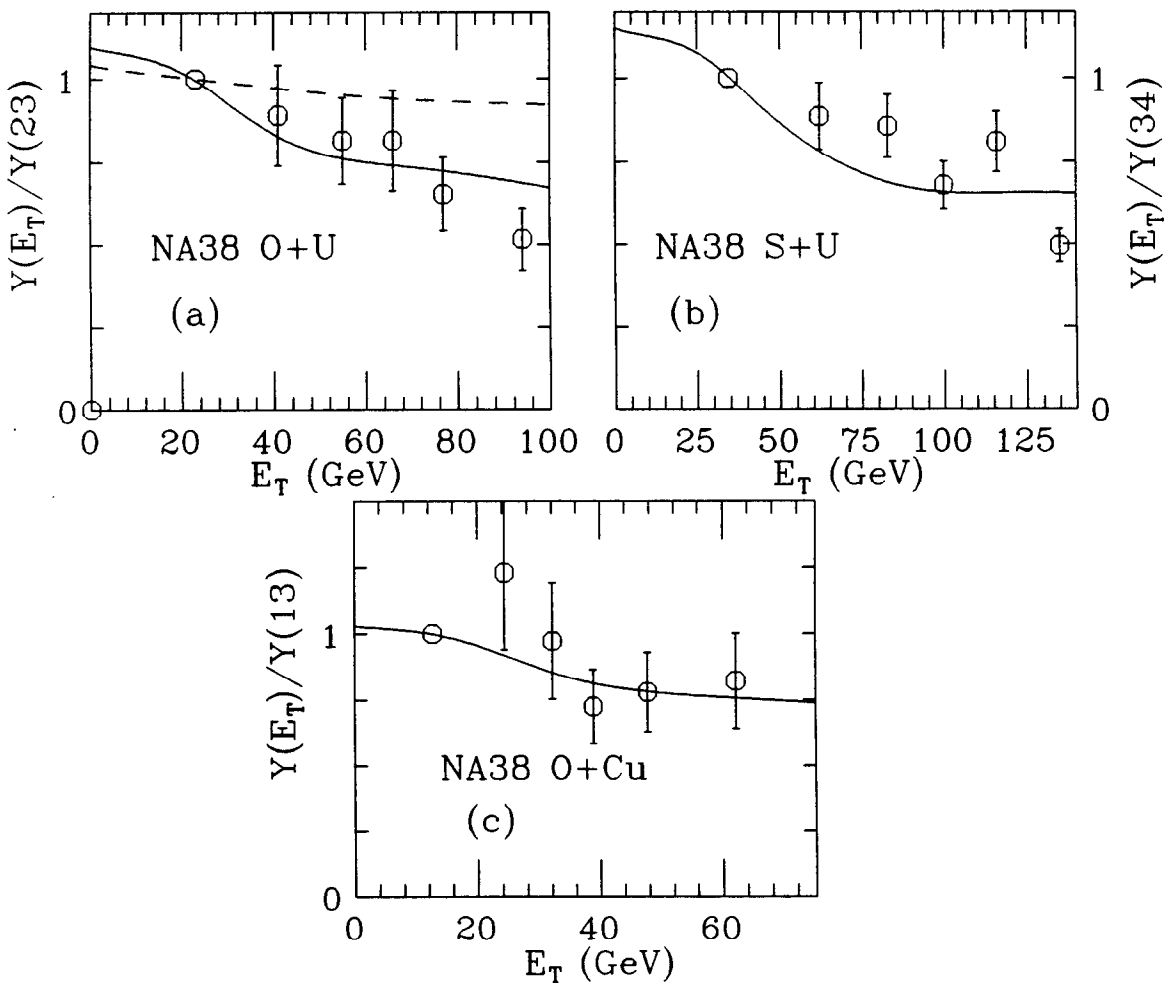
Y(E_T)/Y(23)
NA38 O+U
(a)
0
20
40
60
80
100
E_T (GeV)
Y(E_T)/Y(34)
NA38 S+U
(b)
0
25
50
75
100
125
E_T (GeV)
Y(E_T)/Y(13)
NA38 O+Cu
(c)
0
20
40
60
E_T (GeV)
1
0

Fig. 2

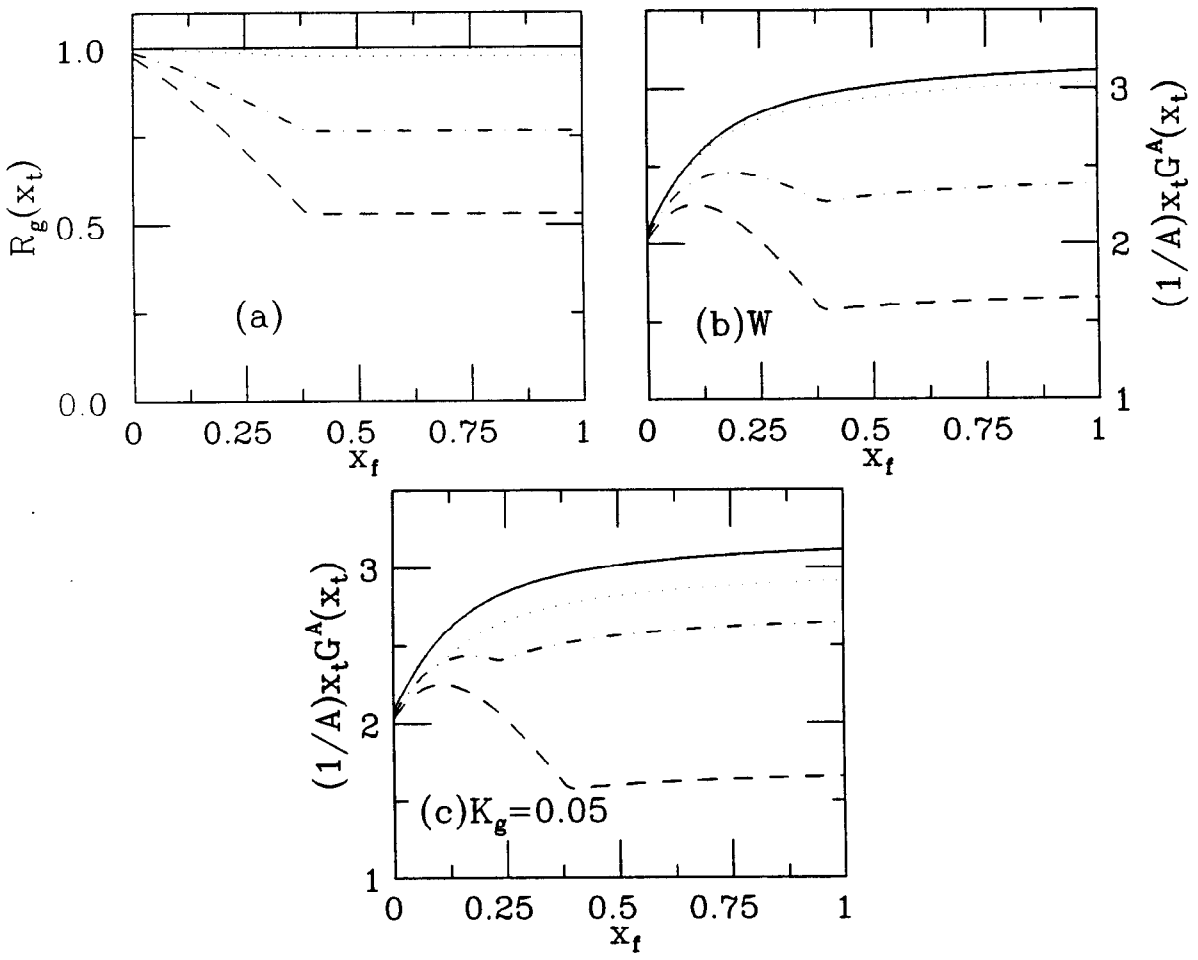

Fig. 3

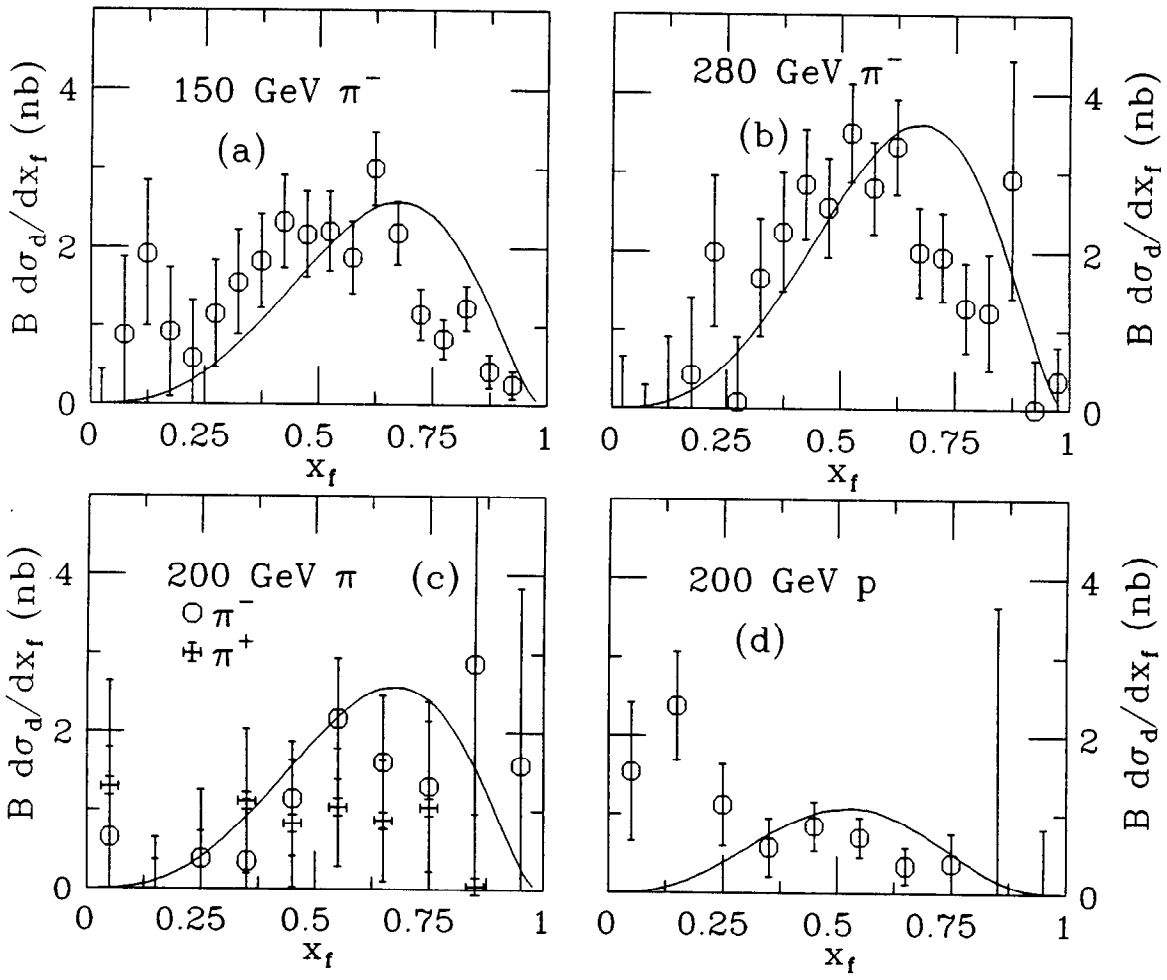
150 GeV π⁻
(a)
280 GeV π⁻
(b)
200 GeV π
(c)
○ π⁻
⊞ π⁺
200 GeV p
(d)
B dσd/dxf (nb)
xf
0
0.25
0.5
0.75
1
2
4

Fig. 4

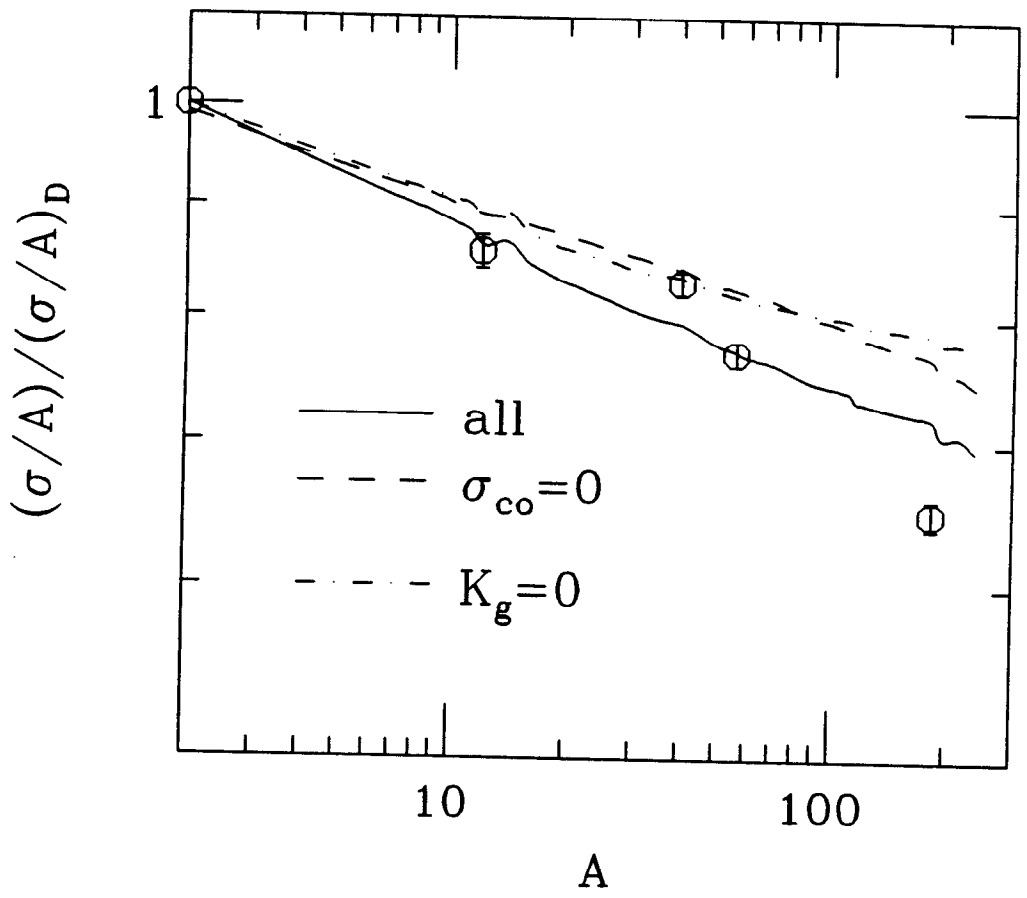

Fig. 5

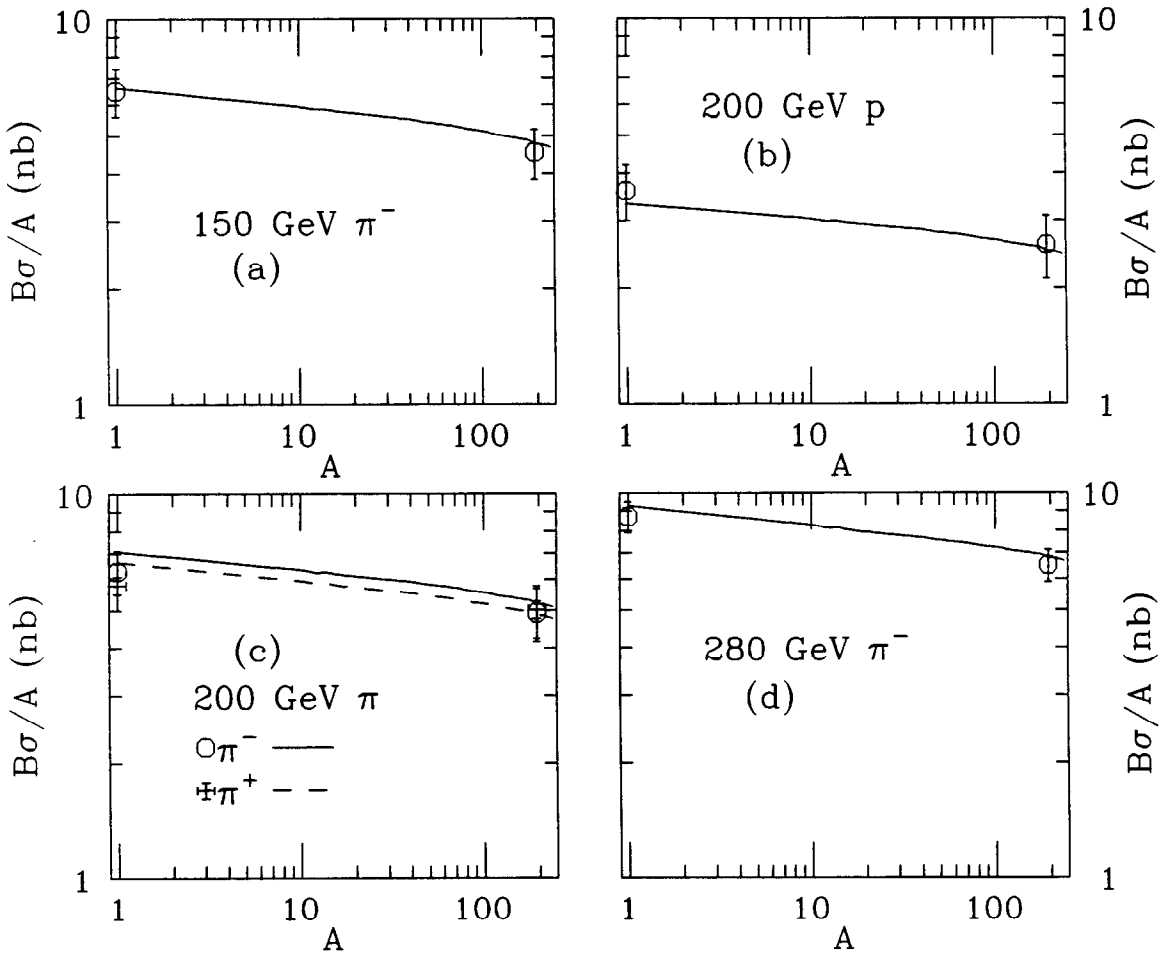

Fig. 6

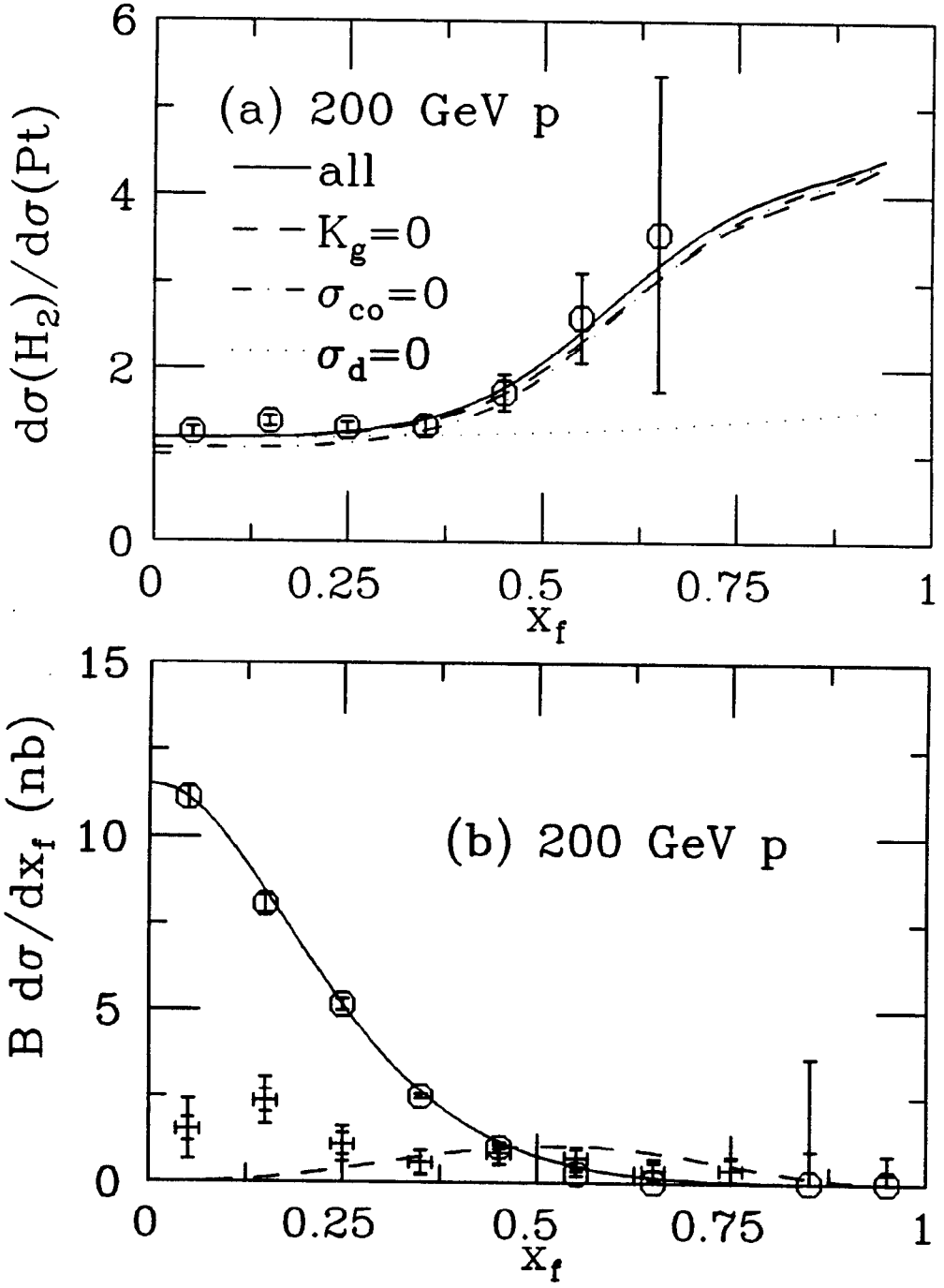
(a) 200 GeV p
all
$K_g=0$
$\sigma_{co}=0$
$\sigma_d=0$
$d\sigma(H_2)/d\sigma(Pt)$
x_f
(b) 200 GeV p
B $d\sigma/dx_f$ (nb)
x_f

Fig. 7

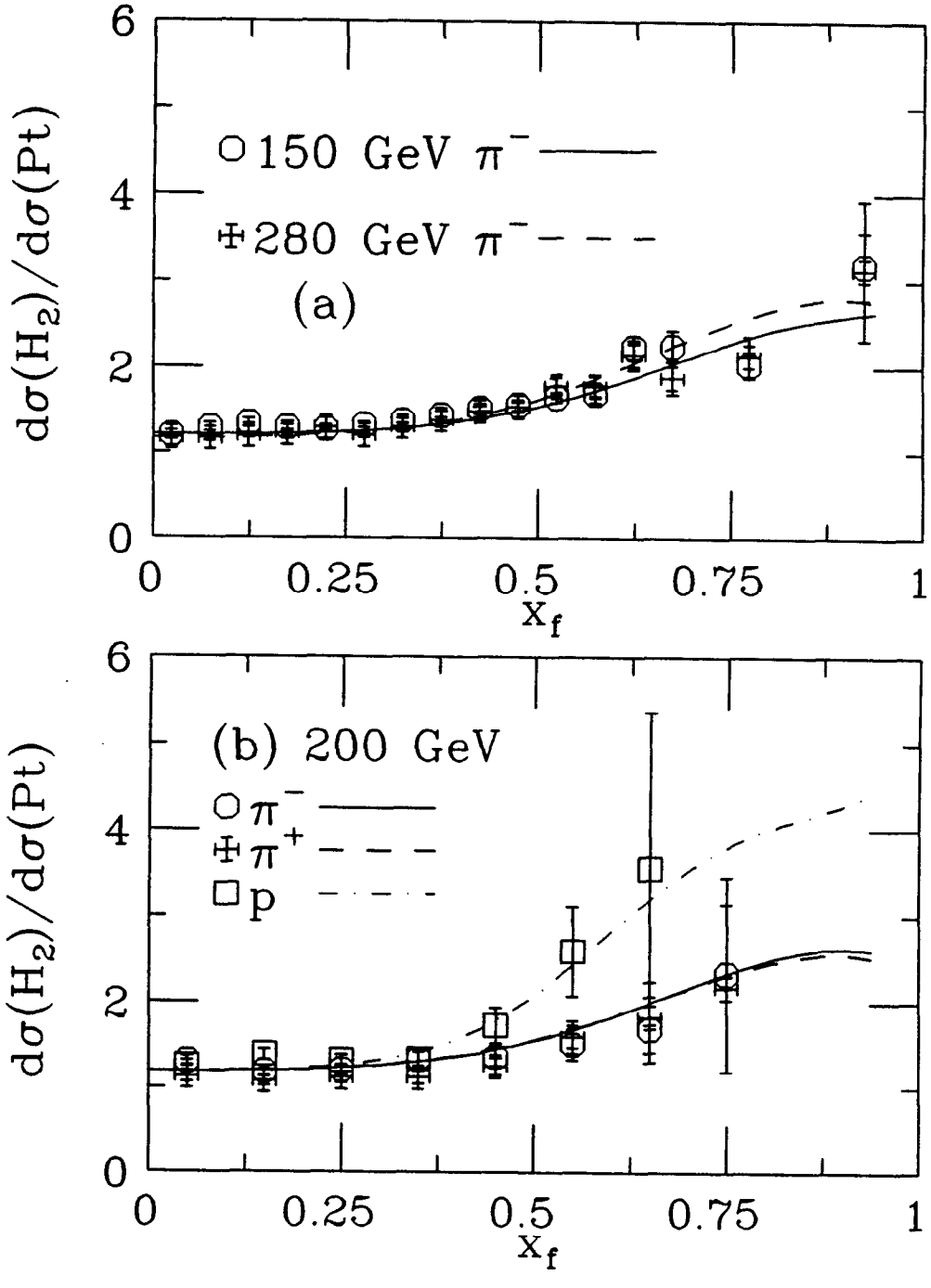
6
4
2
0
0
0.25
0.5
0.75
1
x_f
$d\sigma(H_2)/d\sigma(Pt)$
150 GeV π^-
280 GeV π^-
(a)
(b) 200 GeV
π^-
π^+
p

Fig. 8

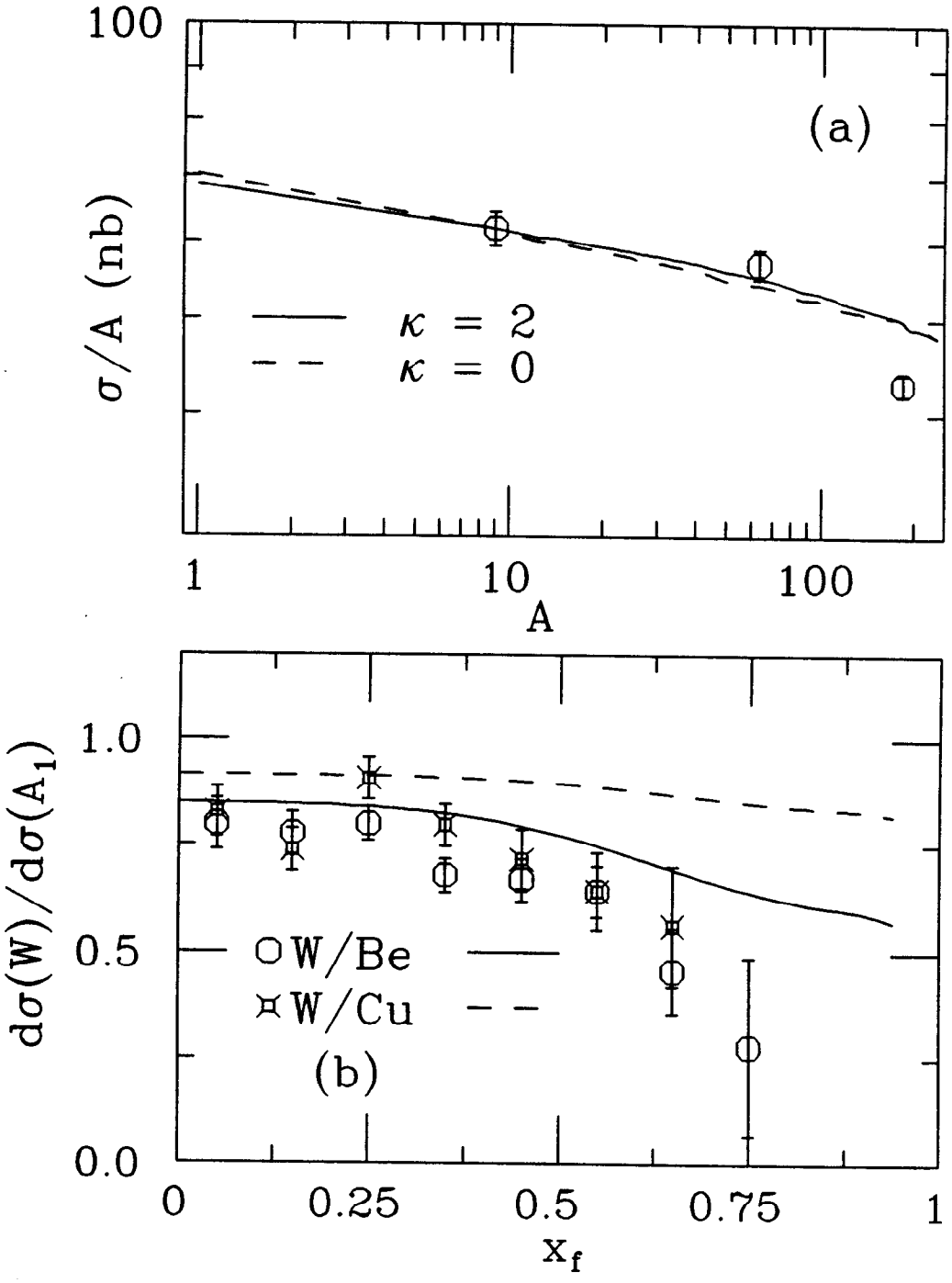
100
(a)
σ/A (nb)
κ = 2
κ = 0
1
10
100
A
1.0
0.5
0.0
dσ(W)/dσ(A1)
W/Be
W/Cu
(b)
0
0.25
0.5
0.75
1
xf

Fig. 9

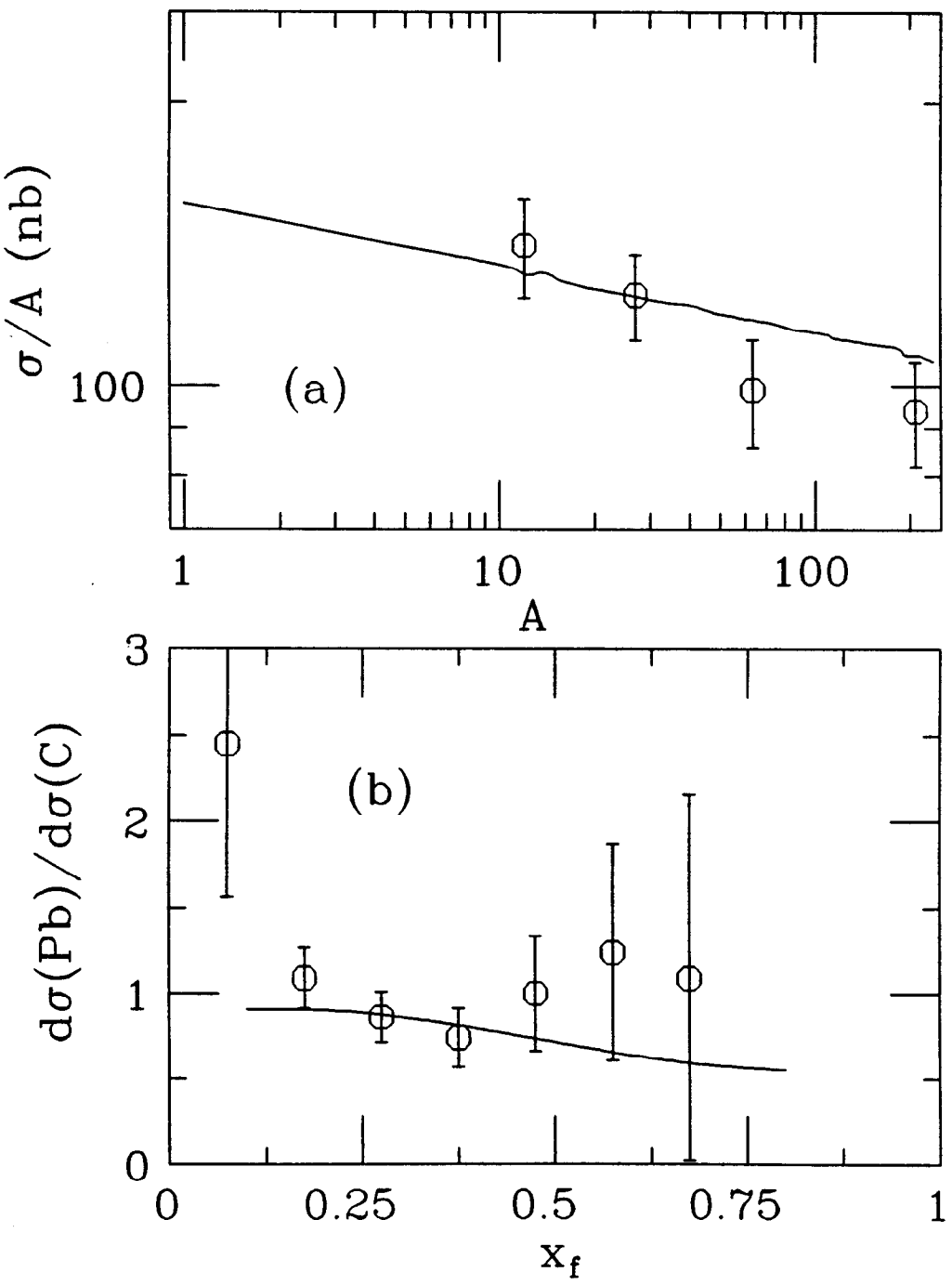

Fig. 10

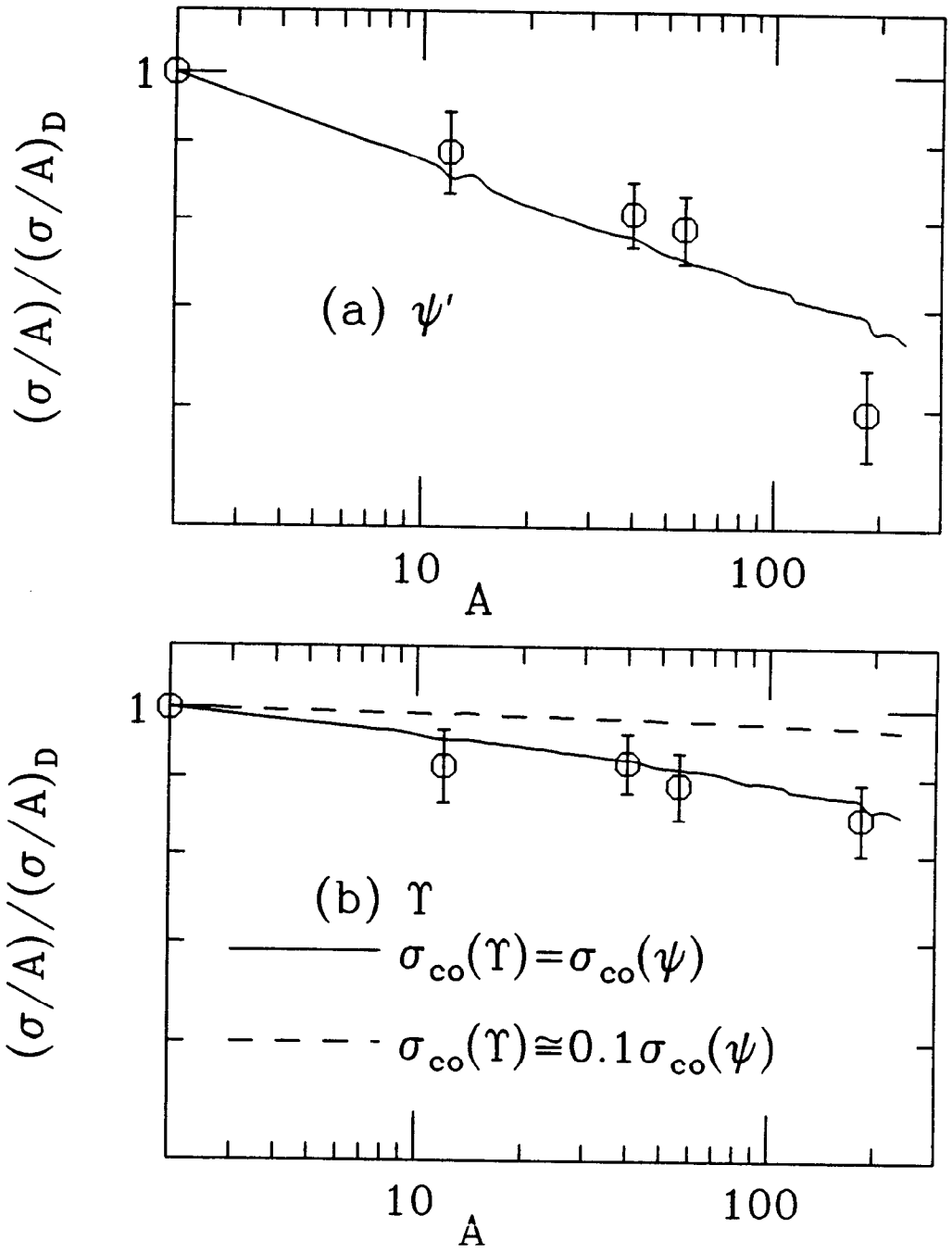

Fig. 11

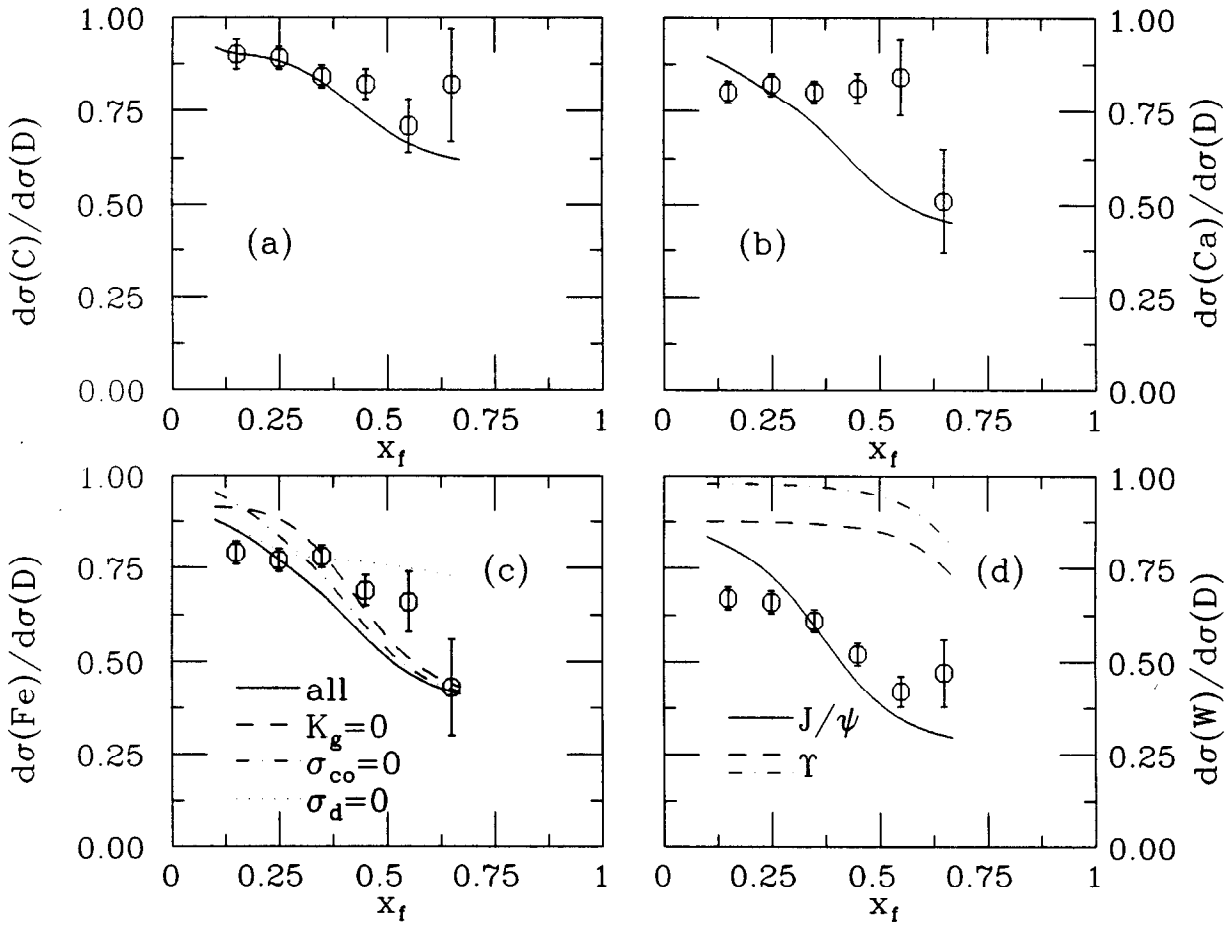
1.00
0.75
0.50
0.25
0.00
0
0.25
0.5
0.75
1
x_f
$d\sigma(C)/d\sigma(D)$
(a)
$d\sigma(Ca)/d\sigma(D)$
(b)
$d\sigma(Fe)/d\sigma(D)$
(c)
all
$K_g=0$
$\sigma_{co}=0$
$\sigma_d=0$
$d\sigma(W)/d\sigma(D)$
(d)
J/ψ
Υ

Fig. 12

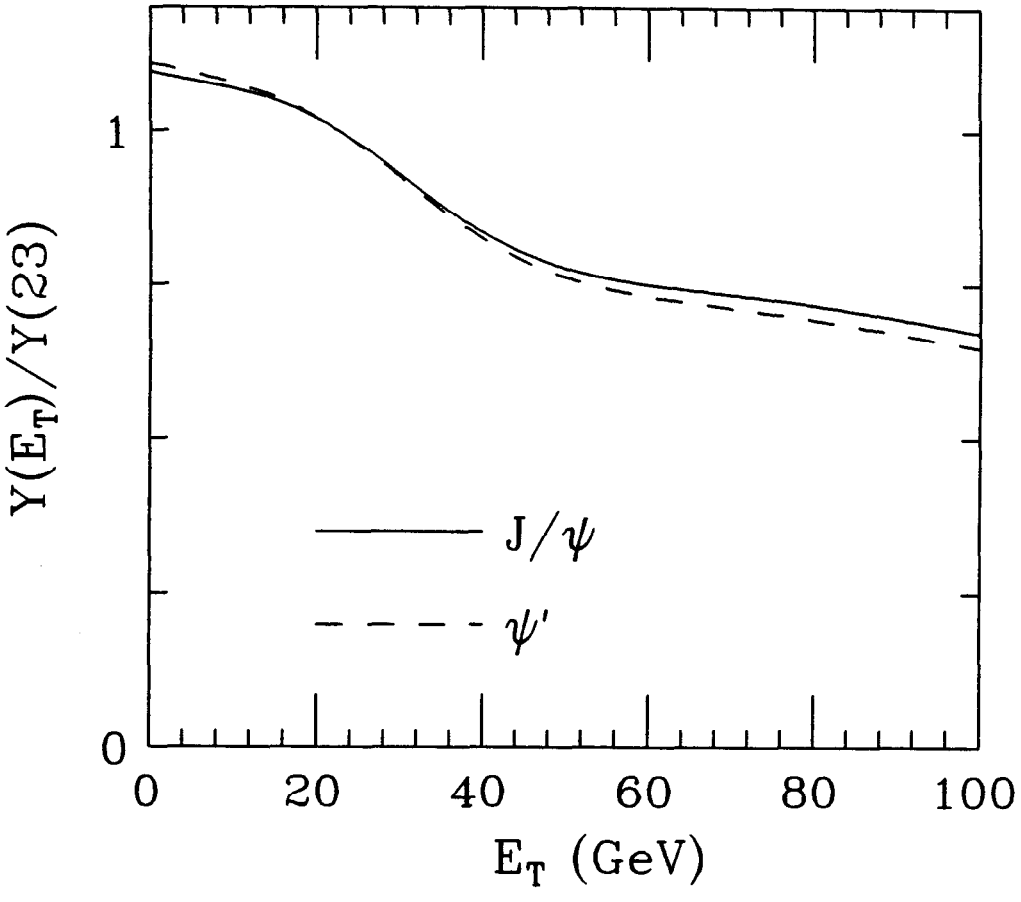

Fig. 13

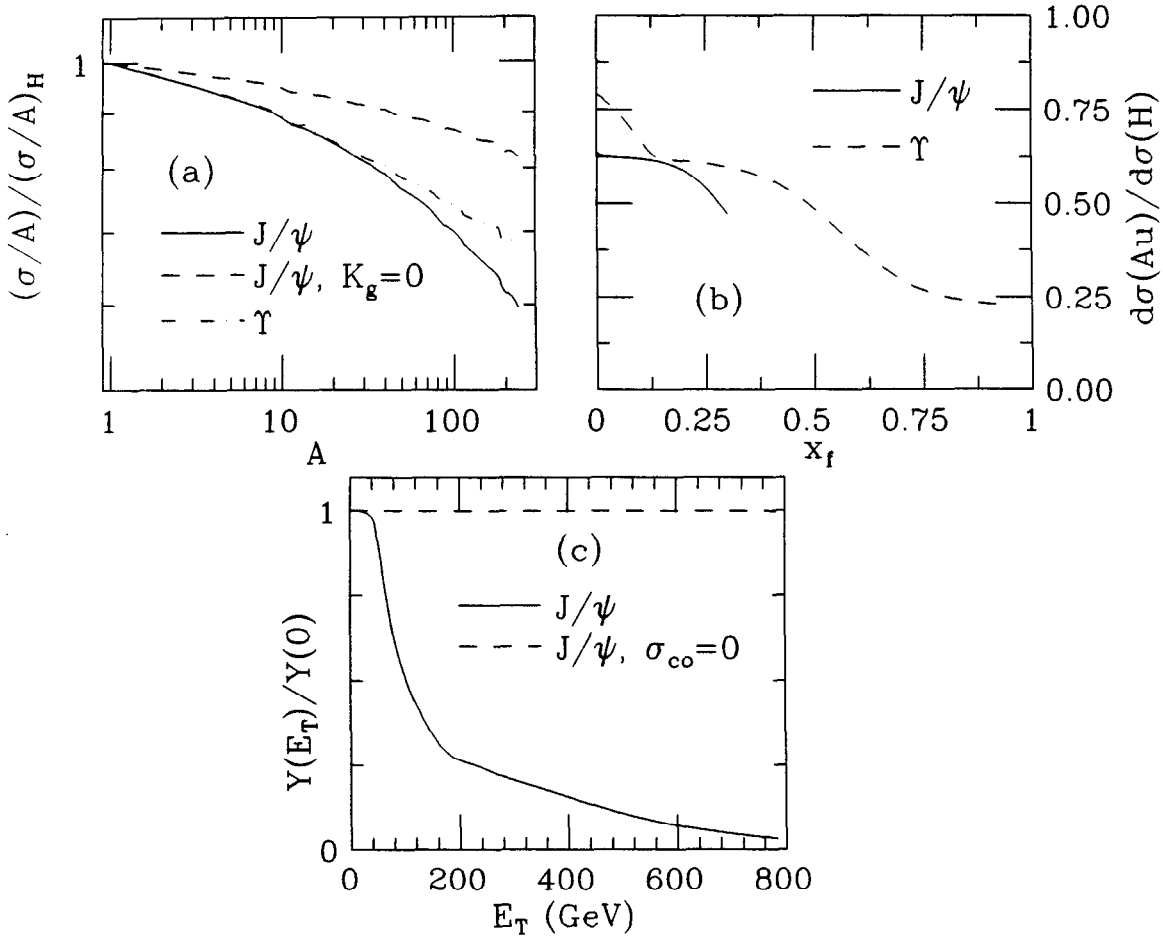
(σ/A)/(σ/A)H
1
(a)
J/ψ
J/ψ, Kg=0
ϒ
1
10
100
A
(b)
J/ψ
ϒ
0
0.25
0.5
0.75
1
xf
1.00
0.75
0.50
0.25
0.00
dσ(Au)/dσ(H)
(c)
J/ψ
J/ψ, σco=0
Y(ET)/Y(0)
1
0
0
200
400
600
800
ET (GeV)

Fig. 14